TRACKING ERRORS AND OPTICAL SCATTER IN A SOLAR TRACKER WITH LINEAR REGRESSION ERROR CORRECTION

by: Norman B. Wood and Stephen K. Cox

Department of Atmospheric Science
Colorado State University
Fort Collins, CO 80523

Funding Agencies:

- National Aeronautics and Space Administration
  (Grant No. Nag 1-1704)
- Office of Naval Research
  (Contract No. N00014-91-J-1422)
- Department of Defense Center for Geosciences Phase II
  (Contract No. DAAH04-94-G-0420)

Colorado State University

DEPARTMENT OF ATMOSPHERIC SCIENCE

PAPER NO. 663

"TRACKING ERRORS AND OPTICAL SCATTER IN A SOLAR TRACKER WITH LINEAR REGRESSION ERROR CORRECTION"

Norman B. Wood and Stephen K. Cox

Department of Atmospheric Science
Colorado State University
Fort Collins, CO 80523

Research Supported by

National Aeronautics and Space Administration (Grant No. NAG 1-1704)

Office of Naval Research (Contract No. N00014-91-J-1422)
and
Department of Defense Center for Geosciences Phase II

(Contract No. DAAH04-94-G-0420)

March, 1998

Atmospheric Science Paper 663

ABSTRACT

TRACKING ERRORS AND OPTICAL SCATTER IN A SOLAR TRACKER WITH LINEAR REGRESSION ERROR CORRECTION

Tracking errors were assessed for a computer controlled solar tracker. The effects of optical scattering on radiometric measurements performed with the tracker were also evaluated. As the position of the tracker is iteratively corrected over time, linear regression is used to calculate a best-fit correction for tracking error. The performance of the tracker was found to be sensitive to the timing of the iterative corrections and to the errors associated with those corrections. Using an optimized scheme for iterative corrections in a field test, the average tracking error was found to be 0.11 ± 0.05 degrees for 48 hours following the final iterative correction.

The solar tracker may be fitted with a mirror which can reflect the image of a target into an instrument. Because the mirror is exposed to multiple sources of illumination (direct sunlight, skylight, and light from surrounding objects) the scattering properties of the mirror are important. The intensity of light scattered from the mirror was compared with the intensity of diffuse skylight. Scatter from the diffuse field incident on the mirror (background scatter) was found to be more significant than scatter from the direct solar beam, and both were significant compared to the intensity of diffuse skylight. Background scatter ranged from 20% to 70% of the total measured signal, depending on

scattering geometry and wavelength. Solar scatter ranged from 1% to 20%, also depending on scattering geometry and wavelength. The scattering properties of the mirror, as measured by the bidirectional reflectance distribution function, appeared to be anisotropic, possibly because of surface defects. For the wavelengths examined, the scattering properties did not follow the wavelength scaling law predicted by Rayleigh-Rice theory for clean, smooth, front-surface reflectors.

ACKNOWLEDGEMENTS

Dr. John Davis and Dave Wood assisted us greatly, providing both advice and helping hands with the solar tracker. We'd also like to thank Chris Cornwall, who performed much of the original development work on the solar tracker, and Melissa Tucker, who assisted in the preparation of a number of earlier versions of this document. This research was supported by the National Aeronautics and Space Administration under contract NAG 1-1704; the Office of Naval Research under contract N00014-81-J-1422, P00007; and the Department of Defense Center for Geosciences Phase II under contract DAAH04-94-G-0420.

TABLE OF CONTENTS

1. Introduction

A number of areas of atmospheric radiation research benefit from high-quality solar radiation measurements at the surface, including:

- studies of the surface energy budget
- studies of the energy budget for the lower atmospheric boundary
- verification of radiation algorithms in numerical models, and
- remote sensing.

While the energy budgets may be evaluated to first order using instruments with hemispheric fields of view, more precise evaluations require observation of the direct component alone; this requires accurate tracking of the sun. The purpose of this research is to develop and test a solar tracking system which will be used in research investigations in the four areas noted above.

1.1 *Instrumentation Requirements*

To accurately measure the directional variation in a radiance field, the orientation of the instrument must be accurately controlled so that it samples the required portion of the field. For example, a normal incidence pyrheliometer must point directly at the sun. A radiometer with a narrow field of view might be used to measure the radiance of a point in a cloud at a fixed angular separation from the sun. In both of these applications, an accurate tracking system is required.

When a tracking system is deployed in the field, accurate tracking becomes a problem. Although the sun's position may be predicted with fairly high accuracy relative to the local coordinate system, it is difficult to align a tracker with this coordinate system. Typically, iterative manual corrections are made to the tracker's alignment over the course of a day's operation. With luck, these iterative corrections result in an optimum setup and accurate tracking. More commonly, this method results in accurate solar tracking only around the time of day of the most recent adjustment.

An additional problem is that an instrument may be too large to mount on a field-deployable tracker. In this case, a mirror may be used to reflect the radiance from the target into the instrument. In this configuration, a mirror mounted on the tracker essentially becomes an external element in the instrument's optical path. However, unlike the other internal elements, the mirror is exposed to extraneous light sources. Since a mirror is not perfectly specular, a portion of this extraneous light may be scattered into the path to the instrument's detector, contaminating the desired signal.

A desirable tracker, then, would be portable and easily deployable in the field. It should forgive moderate inaccuracies in its alignment. Its tracking accuracy should be sufficient to insure that targets are kept within the instrument's field of view. It should be usable with large instruments which are too heavy to mount in the tracker directly. In this mode, it should not introduce significant contamination of the desired measurement. Finally, its position should be easily correctable.

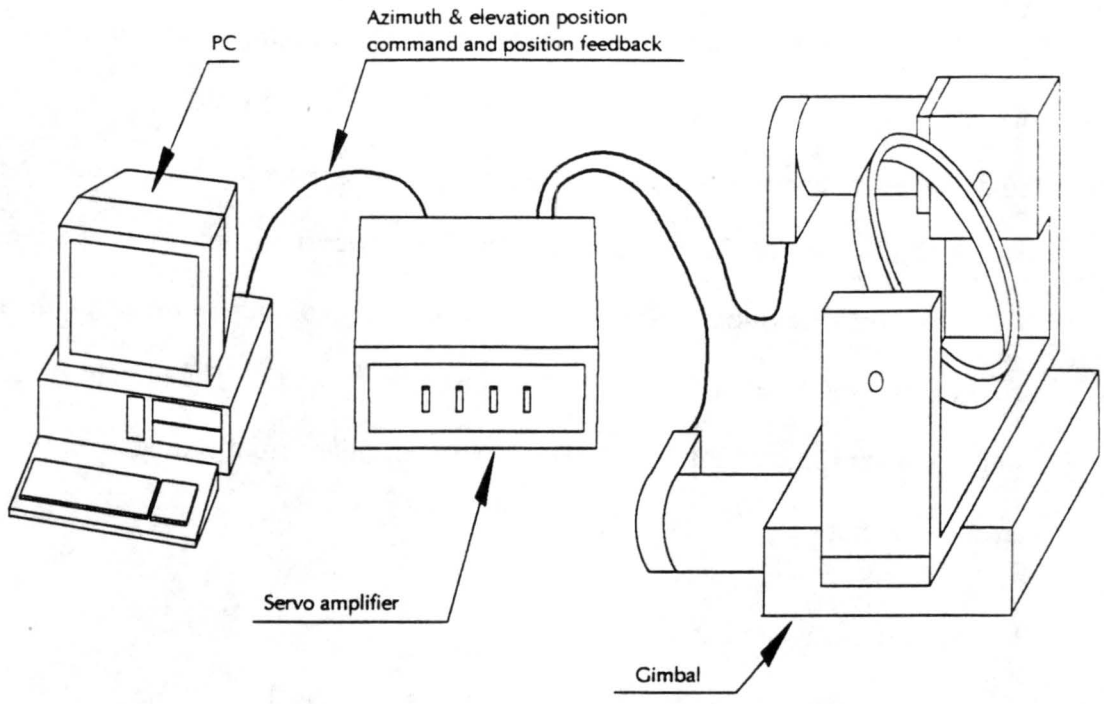

Figure 1: Schematic diagram of solar tracker components

1.2 *The Solar Tracking System*

The tracking system discussed here is described more fully elsewhere (Wood *et al.*, 1996). Relevant excerpts are included in Appendix 1. A short description is included here, insofar as it relates to the work that follows. The tracking system includes a two-axis gimbal optical mount driven with servo motors, servo motor amplifiers, and a personal computer equipped with a two-axis motor controller card (Figure 1). A two-axis mount was used for two reasons. First, the azimuth-elevation nature of the mount translates easily into azimuth-elevation solar position data. Second, a two-axis mount allows for the two modes of operation described above: a direct mode with instruments mounted directly on the gimbal, and a mirror mode in which a mirror is mounted on the gimbal.

Each of the two servo motors used to drive the mount is equipped with an optical encoder for position indication and feedback. The encoders have an absolute resolution of 1,000 counts per encoder revolution and quadrature is used to increase this to 4,000 counts. The gear trains used on the azimuth and elevation stages of the gimbal give a reduction of 54:1. The final resolution is then 216,000 counts per revolution of the azimuth or elevation axis (600 counts per degree) (Aerotech, Inc., 1991). The motors are controlled using a Motion Engineering MC-200 two-axis controller card installed in an IBM AT personal computer.

The computer software includes:

- a routine to calculate the true solar coordinates as a function of time and location on the earth,
- interfaces to the motor control software libraries,
- routines needed to make iterative, manual adjustments to the gimbal position, and
- routines to correct for tracking errors.

The algorithm to calculate the true solar coordinates was adapted from Meeus (1991) and Sax (1991). The motor control libraries were provided by Motion Engineering (1990).

To simplify adjustments for tracking errors, a semi-automated correction method was developed. The method applied in this solar tracker is similar to coordinate transformations used for computer graphics applications and other mathematical transforms (Newman and Sproull, 1979). After setup, iterative corrections are made simply by changing the azimuth and elevation angles of the tracker so that it is pointing directly at the sun. These iterative corrections are made through the computer software. After three iterative corrections are made, one can solve for a transformation matrix

which will convert the true solar coordinates into the coordinates used by the gimbal. True solar coordinates are calculated using the Meeus/Sax astronomical software, then multiplied by the transformation matrix to obtain the gimbal coordinates. While a minimum of three iterative corrections are required, additional corrections allow averaging in a least-squares sense to minimize the effects of random errors in the corrections.

Since the tracker is aimed using explicitly calculated azimuth and elevation angles, a number of tracking modes are possible. In solar mode, the tracker points directly at the sun. In offset mode, the tracker points to a position on the sun's apparent trajectory, but at a fixed temporal offset from the current solar position. For example, for a +5 minute offset, the solar position at (local time + 5 minutes) is calculated, and this is where the tracker is pointed. In scanning mode, angular offsets can be applied separately to azimuth and elevation angles and can be made to vary sinusoidally as a function of time.

1.3 *Objectives*

A number of issues affect the accuracy of measurements made using the tracker. Chief among these is the accuracy of the tracker itself. If the radiance field being measured varies spatially (as might occur when measuring across the forward scattering peak of a parcel containing cloud particles), small errors in the tracker's position can potentially cause large errors in the measured radiance field. If the tracker is to be left unattended for long periods of time, the magnitude of the tracking error as a function of time becomes an issue. For ease of use, it is desirable that the tracker maintain accurate tracking for a period of several hours. For unattended use, the period might extend to a day or longer.

The second, related issue is the numerical behavior of the algorithm used to calculate the transformation matrix. Under some conditions, the algorithm might prove to be excessively sensitive to small errors in the iterative correction points and to the limited precision of the computer's floating point arithmetic. At best, this sensitivity could result in gross errors in the calculation of the transformation matrix. At worst, it could result in numerical errors which might cause the tracking program to crash.

The third issue relates to the scattering effects of the mirror. The mirror itself has a hemispherical field of view. Under typical conditions, the mirror is exposed to two distinct radiance fields: an intense, direct field originating from the sun; and a low-level diffuse field consisting of sky light plus radiance emitted or reflected from the ground and surrounding objects. Two scenarios can be considered for operation in mirror mode. In one scenario, an instrument is positioned to receive the direct solar beam reflected by the mirror. In this scenario, the signal received by the instrument is the specular reflection of the direct solar beam plus light from the diffuse field which has been scattered by the mirror into the instrument's field of view. In most cases, the radiance due to the direct solar beam will be much larger than that due to the mirror-scattered diffuse field, and the scattering effects of the mirror likely can be ignored.

In the second scenario, an instrument is positioned to measure a diffuse radiance reflected by the mirror. For example, a radiometer might be positioned to view, through the mirror, a part of the sky at a few degrees angular separation from the sun. In this scenario, the signal received by the instrument is the specular reflection of the diffuse sky light, plus light from the remainder of the diffuse field which has been scattered by the mirror into the instrument's field of view, plus light from the direct solar beam which has

been similarly scattered into the instrument's field of view. Unlike the first scenario, it is not clear that the desired signal (the specular reflection of the skylight) will be much larger than the other two contributions. The scattering effects of the mirror may not be negligible.

The objectives of the work performed here are then threefold. First, assess the performance of the tracking error correction algorithm. This includes evaluating the numerical stability of the calculation of the transformation matrix and insuring that it remains stable under typical operating conditions. Second, evaluate the performance of the tracking system as a whole in terms of tracking error. Third, examine the effects of the mirror's scattering properties on measurements of the diffuse field.

2. Sources of Tracking Error

Tracking errors can be attributed to a number of causes, primarily:

- misalignment of the gimbal,
- inaccurate calculation of the true solar position, and
- electromechanical errors in the tracking system.

Assuming local horizontal coordinates are being used, misalignment can be partitioned into two distinct sources of error, error in meridional alignment and error in zenith (or level) (Figure 2) . The vertical axis around which the gimbal rotates should be pointed along the local zenith. The horizontal axis around which the gimbal rotates should be

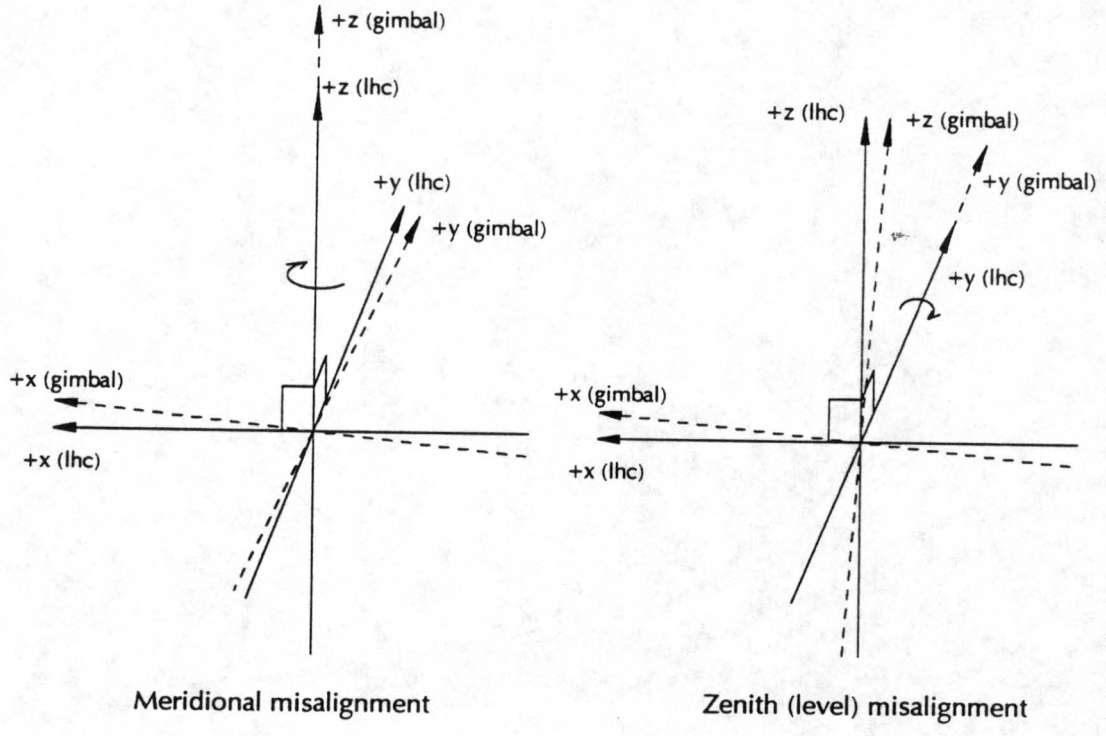

Figure 2: Sources of error in alignment. The figure on the left illustrates a rotation about the z-axis. The figure on the right, a rotation about the y-axis.

normal to the local meridian when the gimbal is pointed north or south, and normal to the vertical axis. Provided the horizontal and vertical axes of the gimbal are normal to each other (this would be controlled by the assembly of the gimbal and is taken to be true) any real misalignment will consist of some combination of error in meridional alignment and error in zenith. The actual, misaligned orientation of the gimbal can then be related to the ideal orientation by a simple rotation about some axis (Figure 3). If the error were strictly an error in meridional alignment, the rotation axis would be vertical. If the error were strictly an error in zenith, the rotation axis would lie somewhere in the horizontal plane. The coordinate systems used to define the true local horizontal coordinates and the gimbal's coordinates are defined in more detail below.

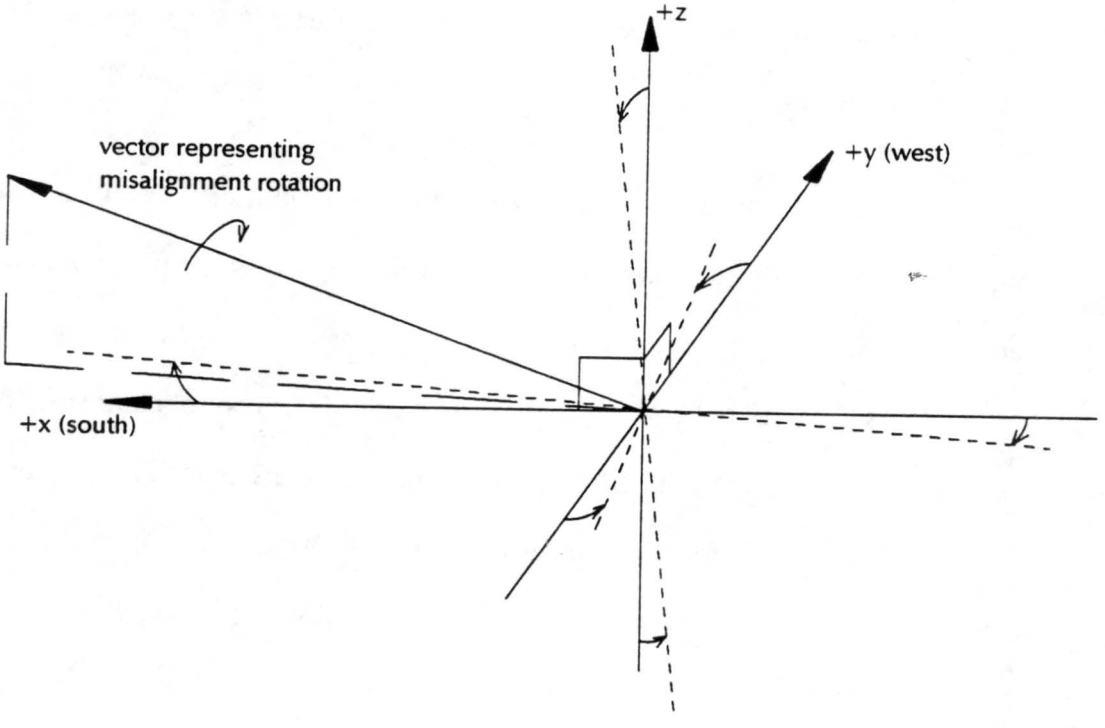

Figure 3: Misalignment defined by rotation about an arbitrary axis.

Calculation of the true solar position requires that a number of parameters be accurately known. These parameters include the observer's location on the earth (latitude, longitude and altitude), the date, the time, and the effects of atmospheric refraction. Provided these quantities are accurately known, the accuracy of the calculation of the true solar position depends on the approximations used in the calculation algorithm. In the field, the observer's location can usually be determined using a global positioning system (GPS) receiver. Synchronization with coordinated universal time (UTC) to within one second can be readily achieved either through the GPS signal or through National Institute of Standards and Technology broadcasts from station WWV. The effects of atmospheric refraction can also be approximately calculated. However, refraction is negligible over most of the sky, ranging from zero degrees when the zenith angle is zero, to 0.1 arcminutes when the zenith angle is 45 degrees, and to 35 arcminutes when the zenith angle is 90 degrees (Meeus, 1991). In this work, the effects of atmospheric refraction have been neglected.

Two sources of error occur in the electromechanical system (*i.e.*, the servo motor amplifiers, the servo motors, and the gimbal). The first, the servo error, arises when the servo motor position deviates from the position commanded by the control software. The servo error is expected to be mainly a function of the motor control parameters (gain, pole, zero) and the load on the gimbal. The second, the mechanical error, occurs when, because of looseness or friction in the drive train, the position of the gimbal does not match that of the servo motors. The mechanical error is expected to be mainly a function of the fit of the drive train and the load on the gimbal.

3. Compensation for Misalignment

Assuming one can determine the true solar coordinates with sufficient accuracy, and that the electromechanical errors in the tracker are negligible, tracking errors can be attributed to misalignment. This section describes the geometry and mathematics involved in the misalignment problem and the techniques used to compensate for misalignment.

3.1 *The Transformation Matrix*

As described in Wood *et al.* (1996), two different coordinate systems must be overlaid: the local horizontal coordinate system, in which the true solar coordinates are calculated using astronomical software, and the gimbal coordinate system, which is defined by the initial setup of the gimbal. Both coordinate systems are represented as three-dimensional cartesian coordinates, sharing a common origin, with axes defined in a left-handed sense. For the local horizontal coordinates, positive x is to the south, positive y is to the west, and positive z is vertical. The gimbal coordinates have a similar orientation, but are not perfectly aligned with the local horizontal coordinates.

Since the two coordinate systems are cartesian and share the same origin, an arbitrary position in the local horizontal coordinates can be transformed to a position in the gimbal coordinates through the use of a single 3×3 transformation matrix. Thus, once the transformation matrix is known, the true solar coordinates are multiplied by the transformation matrix, giving the sun's position in the gimbal coordinate frame. The gimbal can then be moved to the required position.

In cartesian coordinates, an object's position in the ***l***ocal ***h***orizontal ***c***oordinates (***lhc***) can be represented by a vector:

$$\boldsymbol{x}_{lhc} = \left[x_{lhc}, y_{lhc}, z_{lhc} \right] \tag{1}$$

as can the object's position in ***gim***bal coordinates:

$$\boldsymbol{x}_{gim} = \left[x_{gim}, y_{gim}, z_{gim} \right] \tag{2}$$

The transformation from local horizontal coordinates to gimbal coordinates can be accomplished by multiplying $\boldsymbol{x}_{lhc}$ by the 3×3 transformation matrix, $\boldsymbol{A}$:

$$\boldsymbol{x}_{gim} = \boldsymbol{x}_{lhc} \cdot \mathbf{A} \tag{3}$$

Given known values for $\boldsymbol{x}_{lhc}$ and $\boldsymbol{x}_{gim}$, the equation may be solved for $\boldsymbol{A}$. If only a single pair of vectors $\boldsymbol{x}_{lhc}$ and $\boldsymbol{x}_{gim}$ is known, the matrix $\boldsymbol{A}$ is under-determined. However, once three or more distinct pairs of $\boldsymbol{x}_{lhc}$ and $\boldsymbol{x}_{gim}$ are known, a solution for $\boldsymbol{A}$ is possible. Let $\boldsymbol{X}_{lhc}$ and $\boldsymbol{X}_{gim}$ be matrices containing multiple instances of $\boldsymbol{x}_{lhc}$ and the corresponding $\boldsymbol{x}_{gim}$, respectively:

$$\mathbf{X}_{lhc} = \begin{bmatrix} x_{lhc,1} & y_{lhc,1} & z_{lhc,1} \\ x_{lhc,2} & y_{lhc,2} & z_{lhc,2} \\ \cdot & \cdot & \cdot \\ \cdot & \cdot & \cdot \\ x_{lhc,N} & y_{lhc,N} & z_{lhc,N} \end{bmatrix} \tag{4}$$

and

$$\mathbf{X}_{gim} = \begin{bmatrix} x_{gim,1} & y_{gim,1} & z_{gim,1} \\ x_{gim,2} & y_{gim,2} & z_{gim,2} \\ \cdot & \cdot & \cdot \\ \cdot & \cdot & \cdot \\ x_{gim,N} & y_{gim,N} & z_{gim,N} \end{bmatrix} \tag{5}$$

where N is the number of iterative corrections. When $N = 3$, the transformation equation can be exactly solved for A:

$$\mathbf{A} = \mathbf{X}_{lhc}^{-1} \cdot \mathbf{X}_{gim} \tag{6}$$

3.1.1 The Effects of Uncertainty

In reality, neither X_{lhc} nor X_{gim} are known exactly. The elements of X_{lhc} are obtained from calculations of the solar position by the astronomical software and so are subject to any errors in the model used to develop the calculations. The matrix X_{gim} can also only be approximated. The position of the sun in gimbal coordinates is obtained each time the operator makes an iterative correction to point the tracker at the sun. Once such a correction is made, the gimbal position is read from the optical encoders. Since errors exist in each iterative correction, some errors also exist in the sun's gimbal coordinates. Equation (6) can thus be rewritten as:

$$\mathbf{A}' = (\mathbf{X}_{lhc} + \varepsilon_{lhc})^{-1} \cdot (\mathbf{X}_{gim} + \varepsilon_{gim}) \tag{7}$$

where A' represents an approximation to the transformation matrix, ε_{lhc} is the matrix of errors in the local horizontal coordinates, and ε_{gim} is the matrix of errors in the gimbal coordinates.

As before, when $N = 3$, (7) can be solved exactly for A'. However, because of uncertainty (primarily the measurement errors in X_{gim}), the calculated A' may not be accurate. In particular, if the matrix $(X_{lhc} + \varepsilon_{lhc})$ is somewhat ill-conditioned, its inverse may amplify the errors ε_{gim} when (7) is evaluated, causing A' to be grossly inaccurate.

When $N > 3$, A' is over-determined. The over-determined case probably provides better results, since multiple iterative corrections should reduce the uncertainty in A', provided

a least-squares solution technique is applied to the data. Since errors are associated with both X_{lhc} and X_{gim}, a total least-squares approach is indicated (Van Huffel and Vandewalle, 1991). However, the algorithm used to calculate A' must run quickly, so as not to interfere with the real-time operation of the tracker. Since the errors associated with X_{lhc} (see section 4.1) are small relative to those that might be expected for X_{gim}, a simpler, classical least-squares technique is used.

Ignoring the errors in X_{lhc} and letting $X_{obs} = (X_{gim} + \varepsilon_{gim})$, the matrix form of the transformation equation is:

$$\mathbf{X}_{obs} = \mathbf{X}_{lhc} \cdot \mathbf{A}' \tag{8}$$

A typical method is to calculate A' as:

$$\mathbf{A}' = \left(\mathbf{X}_{lhc}^{T} \cdot \mathbf{X}_{lhc}\right)^{-1} \left(\mathbf{X}_{lhc}^{T}\right)\left(\mathbf{X}_{obs}\right) \tag{9}$$

where X^T_{lhc} is the transpose of X_{lhc}. The inverse term, $(X^T_{lhc} \cdot X_{lhc})^{-1}$, may be evaluated using a number of different techniques, but this approach is prone to problems if $X^T_{lhc} \cdot X_{lhc}$ is ill-conditioned.

To avoid this problem, a technique using singular value decomposition (SVD) is applied. Details of the technique are described in Press *et al.*, (1992) and are summarized here. The matrix X_{lhc}, which is of size $N \times 3$, can be decomposed into the product of an $N \times 3$ column orthogonal matrix U, a 3×3 diagonal matrix W, and the transpose of a 3×3 orthogonal matrix V:

$$\mathbf{X}_{lhc} = \underbrace{\begin{bmatrix} u_{1,1} & u_{1,2} & u_{1,3} \\ u_{2,1} & u_{2,2} & u_{2,3} \\ \cdot & \cdot & \cdot \\ \cdot & \cdot & \cdot \\ u_{N,1} & u_{N,2} & u_{N,3} \end{bmatrix}}_{\mathbf{U}} \cdot \underbrace{\begin{bmatrix} w_1 & 0 & 0 \\ 0 & w_2 & 0 \\ 0 & 0 & w_3 \end{bmatrix}}_{\mathbf{W}} \cdot \underbrace{\begin{bmatrix} v_{1,1}^T & v_{1,2}^T & v_{1,3}^T \\ v_{2,1}^T & v_{2,2}^T & v_{2,3}^T \\ v_{3,1}^T & v_{3,2}^T & v_{3,3}^T \end{bmatrix}}_{\mathbf{V}^T} \tag{10}$$
$$= \mathbf{U} \cdot \mathbf{W} \cdot \mathbf{V}^T$$

The diagonal elements of W, denoted as w_i, are the singular values of X_{lhc}. These are the nonnegative square roots of the eigenvalues of $X^T_{lhc} \cdot X_{lhc}$ (Kincaid and Cheney, 1991).

In order to find the least-squares solution for A', the pseudoinverse of X_{lhc}, denoted as X^+_{lhc}, must be calculated, and is given by:

$$\mathbf{X}^+_{lhc} = \mathbf{V} \cdot \mathbf{W}^{-1} \cdot \mathbf{U}^T \tag{11}$$

Since W is diagonal, the inverse W^{-1} is simply the matrix whose diagonal elements are the reciprocals of w_i. Problems occur if some $w_i = 0$, or if some w_i are near zero. These small values of w_i indicate that X_{lhc} is ill-conditioned. To overcome problems related to the ill-conditioning, the reciprocal $1/w_i$ is replaced by zero if $w_i = 0$ or if w_i is exceedingly small (Press *et al.*, 1992). Finally, A' is calculated as:

$$\mathbf{A}' = \mathbf{X}^+_{lhc} \cdot \mathbf{X}_{obs} \tag{12}$$

3.1.2 Implementation in the Solar Tracking System

Correction points may be collected each time an iterative correction is made to the gimbal's position. In typical operation, the operator sets up, aligns and starts the tracker. Over time, as tracking errors are detected, the operator may switch the tracking software to manual control, then adjust the azimuth and elevation angles until the gimbal is on target. Once the target (typically the sun) is attained, the operator presses a key to signal

the tracking program that the adjustment is complete. The computer records the angular position of the gimbal relative to its home position via the optical encoders mounted on the servo motors. This becomes the observed position. The program then calls the astronomical software to calculate the true solar position in local horizontal coordinates and stores the results. These two positions are stored in a data file, along with any previously collected corrections, as azimuth and elevation angles.

Next, the program checks if sufficient data exist to calculate A'. If so, the program recalls each correction, converts the angular positions into cartesian coordinates by assuming a unit sphere, and stores the results in matrices X_{obs} and X_{lhc}. The SVD least-squares technique described above is then performed to obtain the matrix A'.

After A' is calculated, it may be used to correct for misalignment. The tracking program calculates the true solar position in local horizontal coordinates, then multiplies by A' to obtain the applied coordinates. The gimbal is then moved to the applied coordinates.

3.1.3 Sensitivities

The performance of the error correction algorithm is expected to be sensitive to a number of variables, including:

- magnitude and orientation of misalignment
- errors in the site data (latitude, longitude, altitude, time)
- errors in iterative corrections (*i.e.*, in X_{obs})
- timing and number of iterative corrections
- time of year
- location (primarily latitude) of the tracker

- time lapse between iterative corrections and observations

Errors in the site data should have effects similar to misalignment, but on smaller scale. For example, a one degree error in latitude would be similar to a one degree rotation of the tracker about the y axis. A one degree error in longitude would be similar to a one degree rotation of the tracker about the x axis. Small errors in time or altitude also correspond to alignment errors. Since accurate site data can usually be obtained, and since the resulting errors are similar to misalignment, errors in site data were not considered further.

3.1.4 Tracker Simulation Design

A computer simulation of the tracker was developed to test the effects of the remaining variables on the performance of the correction algorithm. Using the variables listed above as inputs, the simulation marched forward in time, calculating the solar position in both the local horizontal coordinates (true solar position) and in the gimbal coordinates (observed solar position). At any chosen time interval, the simulation could be paused and an iterative correction could be made. After three or more iterative corrections, the transformation matrix was calculated and could be applied to the true solar position. Then the transformed true solar position was compared with the observed solar position.

The magnitude and orientation of the misalignment of the gimbal coordinates with respect to local horizontal coordinates were controlled by specifying a rotation vector (Figure 3). The direction of the vector represents the axis of rotation, while the magnitude of the vector specifies the magnitude of the rotation.

With exception of the numerical stability tests, iterative correction errors were simulated as random deviates normally distributed about a mean of zero so that the mean iterative correction corresponded with the true solar position. A simple central limit theorem approach was used to model the errors (Råde and Westergren, 1990):

$$e = \left[\sum_{i=1}^{12} u_i - 6 \right] \sigma + \mu \tag{13}$$

where e is the simulated iterative correction error, u_i is a series of simulated, uniformly distributed random deviates (obtained from a random number generator), σ is the desired standard deviation for the simulated normal distribution, and μ is the desired mean for the simulated normal distribution. The parameter μ is set to zero and σ is chosen to control the probable size of e. For example, with a true normal distribution, a standard deviation of 0.255 causes the error to fall between ± 0.5 with 95% probability. Thus, the typical magnitude of the errors could be increased or decreased by modifying σ.

For the numerical stability tests, the iterative correction errors were simulated as uniformly-distributed random deviates.

The number and timing of iterative corrections (including the time intervals between corrections) were controlled during operation of the simulation. Iterative corrections could be made at any time during the simulation. The simulation recorded a maximum of thirty iterative corrections and used a minimum time interval of ten minutes. These corrections were stored sequentially and, if more than thirty corrections were made, the earliest corrections were discarded.

The elapsed time between the corrections and the observations was also controlled during operation of the program. The simulation ran forward in time from the start date, up to a maximum of thirty days, but only within the start month. The transformation matrix could be applied to the tracker at any time during the simulation. So, for example, iterative corrections could be recorded during day #1, then several simulated days or weeks later, the transformation matrix could be applied and tracking error measured.

3.1.5 Development of Test Cases

A set of test cases was established to use throughout the testing of the correction algorithm. The cases consisted of:

- moderate misalignment
- varied axes of misaligment
- time of year near an equinox (to obtain a typical 12-hour day)
- mid-latitude, northern hemisphere

The test cases were chosen by running the simulation with no error correction and looking at the tracking error as a function of time. Latitude and longitude were set at 40 degrees N, 105 degrees W, the magnitude of the misalignment was set at 1 degree, and the date was set at 22 September, 1992. The orientation of the rotation axis was varied over elevation angles from 0 degrees to 90 degrees and over azimuth angles from -180 degrees to +180 degrees. The resulting tracking errors were plotted as a function of local time and a set of four typical cases was chosen to use in the remainder of the testing (Figure 4). The test cases, along with the orientations of the misalignment vectors, were:

- Axis A (Elevation 0 degrees, azimuth 0 degrees) - pure zenith misalignment

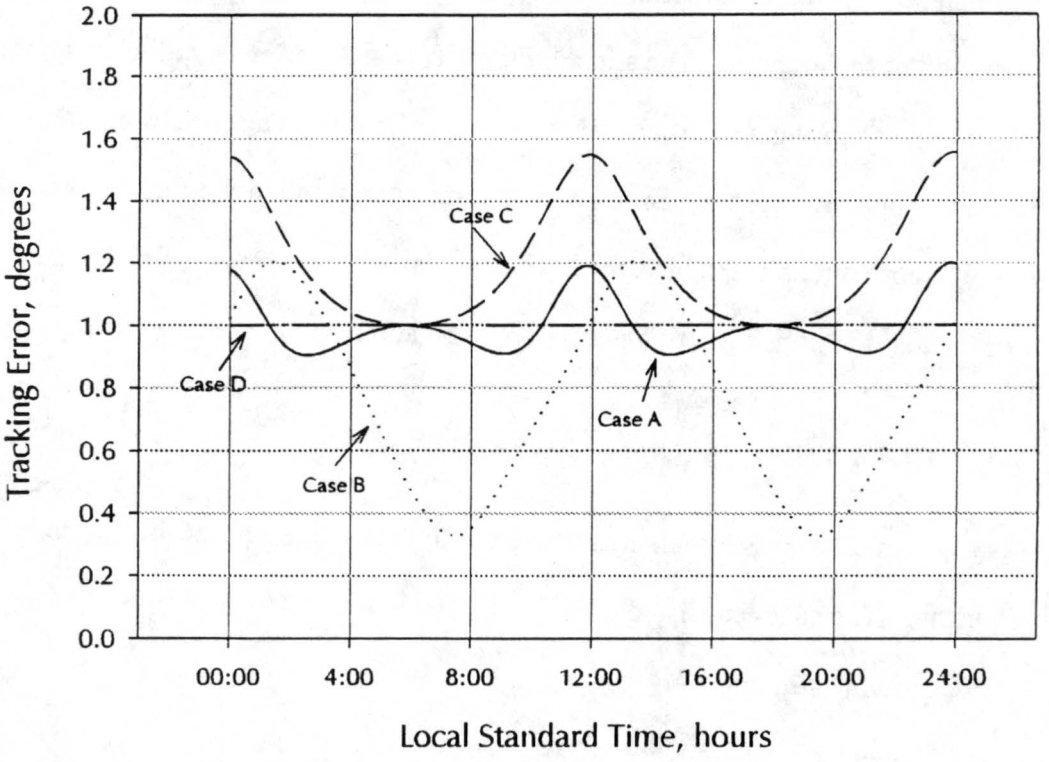

Figure 4: Tracking errors associated with cases used to test the error correction algorithm

- Axis B (Elevation 30 degrees, azimuth -90 degrees) - combined zenith and meridional misalignment
- Axis C (Elevation 45 degrees, azimuth -180 degrees) - combined zenith and meridional misalignment
- Axis D (Elevation 90 degrees) - pure meridional misalignment

3.2 *Numerical Stability Testing*

Initially, the correction algorithm used Gauss-Jordan elimination (GJE) to solve for A', following the method shown in equation (9). Stability problems with the algorithm

occurred when iterative corrections were made at 5-minute or shorter intervals. It wasn't clear whether other situations might create similar stability problems. The GJE version of the correction algorithm was tested by running the simulation for several dates at two-month intervals throughout a year (the 20th day of January, March, May, July, September and November). At each test date, the simulation program was run using test case B with +1.0 degrees rotation. During the first twenty-four simulation hours, corrections were made at 0800, 1200 and 1600 local standard time (LST). The simulation program calculated the transformation matrix, then applied the matrix to the tracker position during the second twenty-four simulation hours. Tracking errors were calculated at intervals of ten simulation minutes throughout each test. The transformation matrices and tracking errors were examined to evaluate the performance of the correction algorithm. In addition, to help assess the cause of the stability problems, condition numbers were calculated for the $X^T_{lhc} \cdot X_{lhc}$ matrices used in the correction algorithm. Matrix condition numbers were calculated using the column-wise *l_1-norm* (Kincaid and Cheney, 1991).

After this testing was completed, the GJE technique was replaced by SVD. The SVD algorithm requires a parameter (which we've called TOL) which measures the smallness of the elements w_i of the diagonal matrix W (see equation 10 and the following discussion). If w_i is smaller than the limit established by this parameter, the reciprocal $1/w_i$ in the inverse W^{-1} is replaced by zero. A series of tests were run with the SVD simulation to determine an appropriate value for this parameter.

First, a benchmark was established by running both the GJE and SVD versions of the simulation to determine an ideal transformation matrix. Test case B was used with +1.0

degree misalignment, a simulation date of 20 March and no errors in iterative corrections. For the SVD simulation, TOL was set to zero. Then, starting at a simulation time of 0630 LST, approximately 24 iterative corrections were made at half-hour intervals. The transformation matrix was calculated (both SVD and GJE versions gave the same result) and this matrix was used as a comparison to evaluate the performance of the SVD version in subsequent tests with different values of TOL.

Next, a series of six SVD simulations was run using the same parameters described above, but with values of TOL ranging from 10^{-6} to 10^{-1}. As above, for each test iterative corrections were made at half-hour intervals starting at 0630 LST. The resulting transformation matrices were compared with that obtained in the benchmark test and an optimum value for TOL was chosen based on the comparisons. This value of TOL was used through all of the subsequent tests.

3.2.1 Results of Numerical Stability Testing

The initial testing of the GJE version of the simulation produced transformation matrices for each of the six simulation dates (Table 1). Also shown (Table 2) are the largest tracking errors occurring during the second simulation day of each test and the condition number for the corresponding $X^T_{lhc} \cdot X_{lhc}$ matrix. To choose a suitable value for TOL, a benchmark transformation matrix was calculated, along with transformation matrices obtained from GJE and from SVD with various values of TOL (Table 3).

3.2.2 Discussion of Numerical Stability Test Results

Given a small misalignment, as was used to perform the numerical stability tests, the transformation matrix should be very close to an identity matrix. For four of the GJE test

Table 1: Numerical stability test results. Transformation matrices calculated using Gauss-Jordan elimination

20 Jan 92:	0.9913	−0.0085	−0.0095
	0.0075	1.0016	0.0048
	0.0337	−0.0009	0.9835
20 Mar 92:	−1.4334	1.7222	0.9148
	0.0052	1.0013	0.0057
	2.0404	−1.4399	0.2289
20 May 92:	0.9968	−0.0150	−0.0284
	0.0106	0.9973	−0.0013
	0.0125	0.0015	1.0061
20 Jul 92:	0.9959	−0.0112	−0.0284
	0.0086	0.9973	−0.0011
	0.0126	0.0011	1.0060
20 Sep 92:	0.5653	0.1212	−0.2384
	0.0112	0.9973	−0.0010
	0.3665	−0.1033	1.1849
20 Nov 92:	1.0093	−0.0121	−0.0060
	0.0090	−0.9976	−0.0015
	−0.0055	0.0139	0.9911

Table 2: Largest tracking errors from numerical stability tests, along with condition numbers for the matrix $X_{lhc}^{T} \cdot X_{lhc}$

Simulation Date	Largest tracking error, degrees	Condition Number
20 Jan 92	1.504	77.25
20 Mar 92	4.800	601,889
20 May 92	0.469	60.68
20 Jul 92	0.406	69.12
20 Sep 92	0.925	29,670
20 Nov 92	2.643	79.06

cases this was true, while in the remaining two cases (March and September) the transformation matrices differed significantly from identity matrices. Thus it appears that the correction algorithm failed to calculate the appropriate transformation matrix. As would be expected if the transformation matrix were inaccurately calculated, the tracking errors for March and September were much larger than in the other cases.

Table 3: SVD tuning results. Selected transformation matrices for benchmark, Gauss-Jordan elimination and SVD with various values of TOL

Benchmark:	0.9998	−0.0087	−0.0151	**GJE Results:**	1.1855	−0.1064	−0.2495
	0.0087	1.0000	−0.0001		0.0081	0.9994	0.0007
	0.0151	−0.0001	0.9999		−0.1429	0.0806	1.1964
TOL = 10^{-1}:	0.4169	−0.0057	0.4858	**TOL = 10^{-3}:**	0.8742	0.1622	0.0472
	0.0076	0.9995	0.0007		0.0082	1.0007	0.0007
	0.5007	−0.0045	0.5835		0.1206	−0.1417	0.9466
TOL = 10^{-5}:	0.5631	0.0487	−0.4954	**TOL = 10^{-6}:**	0.8124	−0.0760	−0.1919
	0.0074	1.0002	−0.0007		0.0079	0.9998	−0.0009
	0.3789	−0.0471	1.3993		0.1701	0.0564	1.1480

The cause of the inaccurate transformation matrices was revealed when the condition numbers were calculated for the $X^T_{lhc} \cdot X_{lhc}$ matrices. The condition numbers for both March and September were much larger than for the remaining cases, indicating that these matrices had a higher degree of ill-conditioning. Larger condition numbers indicate that the solution to an inverse problem is more sensitive to errors in the input data. This increased sensitivity causes the small iterative correction errors to be magnified, resulting in a grossly-erroneous transformation matrix. The timing of the tests (both the March and September tests were near an equinox) appeared to be significant, although this was not explored further.

The SVD tests suggested that a value of 10^{-3} for TOL gave better performance than other values that were tested. This value produced a transformation matrix which most closely matched the benchmark matrix, both in form and in ability to reproduce transformed coordinates.

3.3 *Correction Algorithm Testing*

Once the SVD technique was implemented, four tests were performed to evaluate the sensitivities of the correction algorithm to what were considered to be the most significant (see section 3.1.3) input parameters. The parameters included orientation of misalignment, magnitude of misalignment, magnitude of errors in the iterative corrections, and timing of iterative corrections. Each test was performed by running the simulation for 48 simulation hours using a simulation date of 20 March. Corrections were made during the first simulation day, then the transformation matrix was applied during the second day. Each run was repeated three times (a replicate set) and the average tracking error was calculated at each interval of ten simulation minutes.

- **Orientation of misalignment**

Four replicate sets were performed, one with each of the test cases described in section 3.1.5. The magnitude of the misalignment vector was fixed at 5 degrees. Corrections were made at half-hour intervals between 0630 LST and 1800 LST on the first simulation day.

- **Magnitude of misalignment**

Three replicate sets were performed. The magnitude of the misalignment was varied from 0.5 degrees to 5 degrees to 15 degrees while the rotation axis (Case C: -180 degrees azimuth, +45 degrees elevation) was kept constant. During the first simulation day, corrections were made at half-hour intervals between 0630 LST and 1800 LST.

- **Magnitude of iterative correction errors**

To evaluate the sensitivity to errors in the iterative corrections, three replicate sets were run with varying magnitudes of iterative correction error. The rotation axis (Case C: -180 degrees azimuth, +45 degrees elevation) was kept constant for all three sets, as was the magnitude of the misalignment (5 degrees). During the first simulation day, corrections were made at half-hour intervals between 0630 and 1800 LST. The magnitude of the iterative correction error was controlled by varying the simulation parameter σ. The desired σ for the error model was determined by assuming that the iterative correction errors should fall within a specified range with a specified probability. For example, a 95% probability that the iterative correction errors fall between -0.3 degrees and +0.3 degrees gives a desired σ of 0.153 degrees using a table of the standard normal distribution function (Råde and Westergren, 1990). Similar calculations were made for the σ values used in these tests (Table 4).

- **Timing of iterative corrections**

Four replicate sets were performed, each with different schemes for the timing of iterative corrections. For all four sets, six iterative corrections were made, beginning at 0630 LST, and no corrections were made during nighttime hours. Iterative corrections were made at approximately 30-minute intervals for the first set, 2-hour intervals for the second set, 6-hour intervals for the third set, and 12-hour intervals for the fourth set. The magnitude and orientation of the misalignment (Case B: -90 degrees azimuth, +30 degrees elevation, +5 degrees rotation) was kept constant for all sets. In addition, once these four timing tests were completed, a further test was performed in which an attempt was made to optimize the timing of the corrections.

3.3.1 Results of Correction Algorithm Testing

The performance of the correction algorithm was largely insensitive to changes in the magnitude and orientation of misalignment (Figure 5 and Figure 6). The performance of the correction algorithm was sensitive to the magnitude of the errors in iterative corrections (Figure 7). Tracking errors increased as the parameter σ increased (Table 4) . For each case, the resulting tracking error varied from approximately $\sigma/2$ to $3\sigma/2$.

The performance of the correction algorithm was sensitive to the timing of iterative corrections (Figure 8 through Figure 11). With closely-spaced iterative corrections (Figure 8), the tracking error was weakly periodic with a strong upward trend. The standard deviation of the tracking error remained small. With more broadly-spaced iterative corrections (Figure 9 and Figure 10), the average tracking error was more periodic but had less of an upward trend. However, the standard deviation was larger than with closely-spaced iterative corrections. For iterative corrections spaced at approximately 12-hour intervals (Figure 11), the tracking error was strongly periodic and, although the trend seemed to be flat, the tracking error was larger than in the previous tests.

Table 4: Probable iterative correction error (95% probability) with minimum and maximum tracking errors for various values of sigma

σ degrees	**PROBABLE RANGE OF ITERATIVE CORRECTION ERROR** degrees	**MIN/MAX TRACKING ERROR** degrees
0.01	+/- 0.02	0.00557 / 0.01817
0.10	+/- 0.20	0.08613 / 0.23667
1.00	+/- 2.0	0.52960 / 1.76883

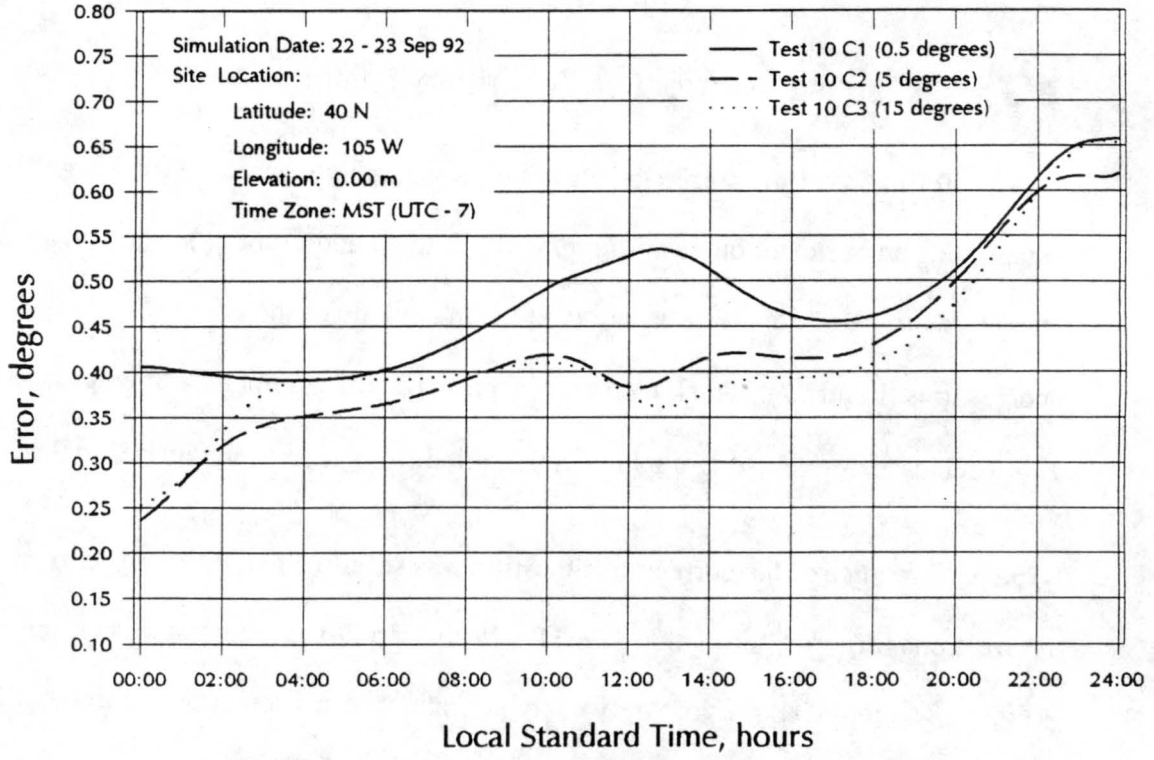

Figure 5: Tracking error for various magnitudes of misalignment

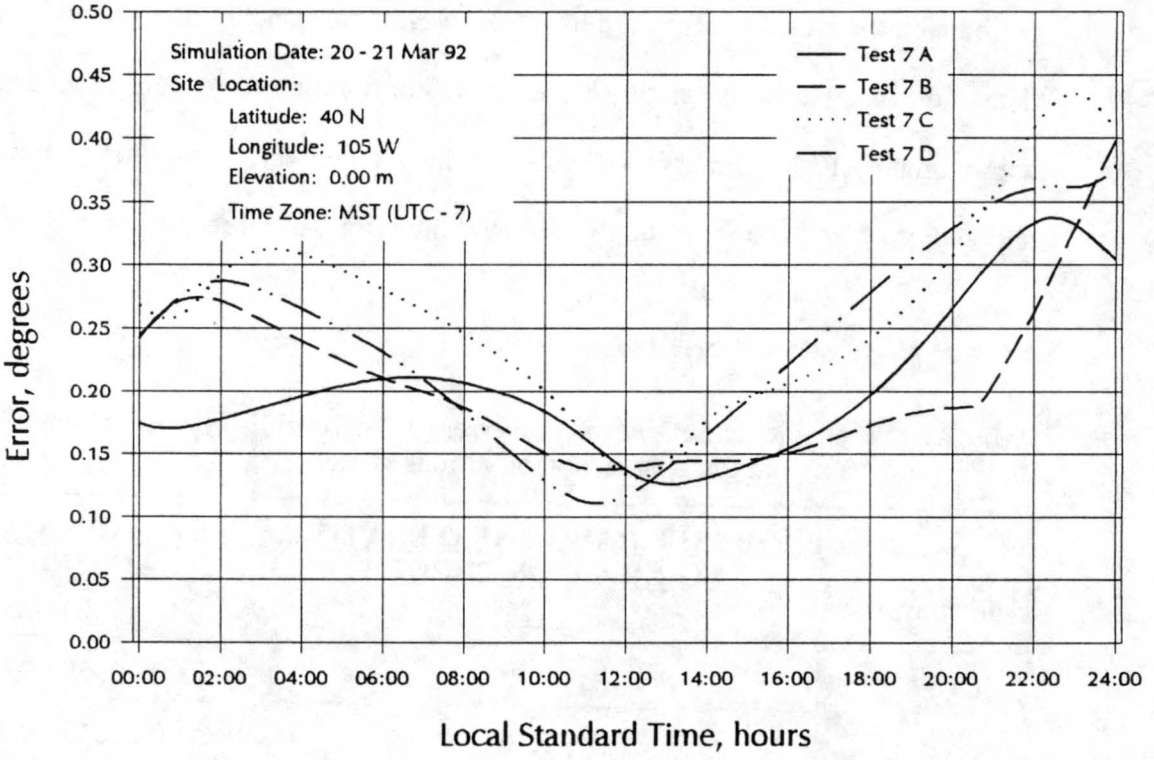

Figure 6: Tracking error for various orientations of misalignment

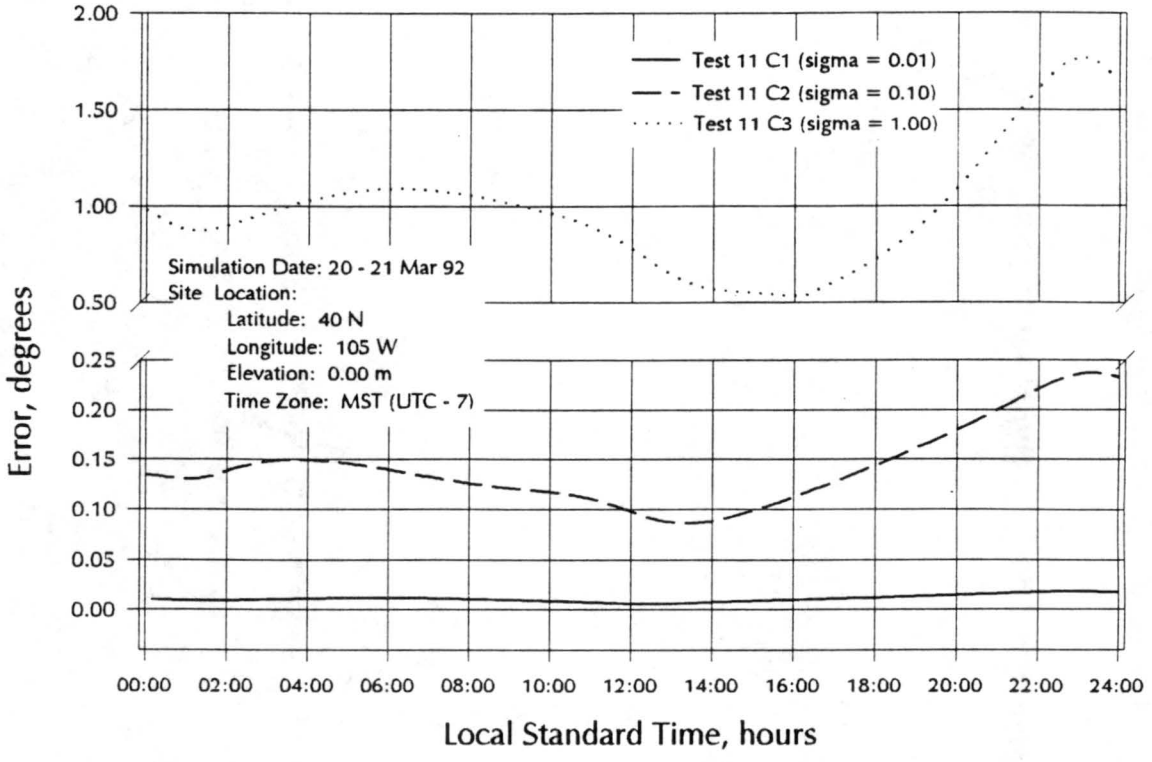

Figure 7: Tracking error for various iterative correction errors

Based on the sensitivity of the correction algorithm to the timing of the iterative corrections, a final scenario was tested in which multiple iterative corrections were made in several clusters distributed throughout the day. A pattern consisting of six clusters at approximately 6-hour intervals (again with no nighttime corrections), with three iterative corrections per cluster, was tested. The average and standard deviation of the tracking error were better than in any previous test (Figure 12). The average tracking error for this test was less than 0.2 degrees after the final iterative correction and remained so for the rest of the test period. The standard deviation was less than 0.1 degrees after the final iterative correction and showed only a slight increasing trend during the remainder of the test.

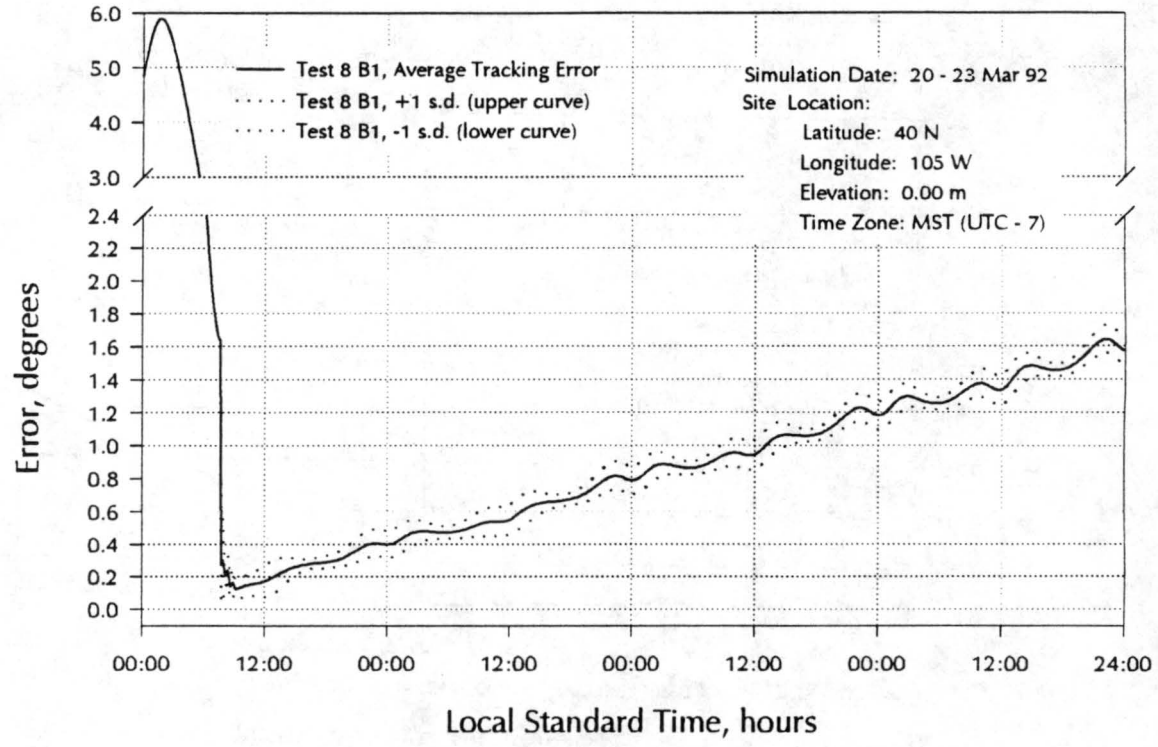

Figure 8: Tracking error for iterative corrections at 30-minute intervals

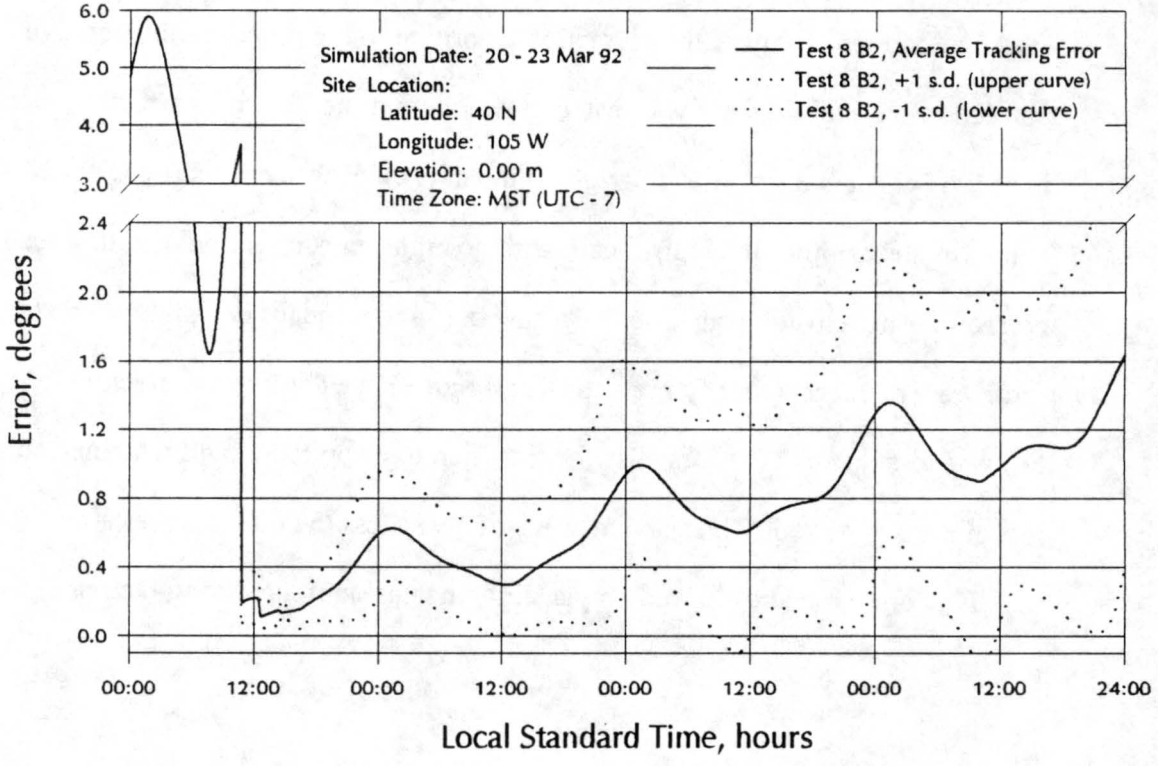

Figure 9: Tracking error for iterative corrections at 2-hour intervals

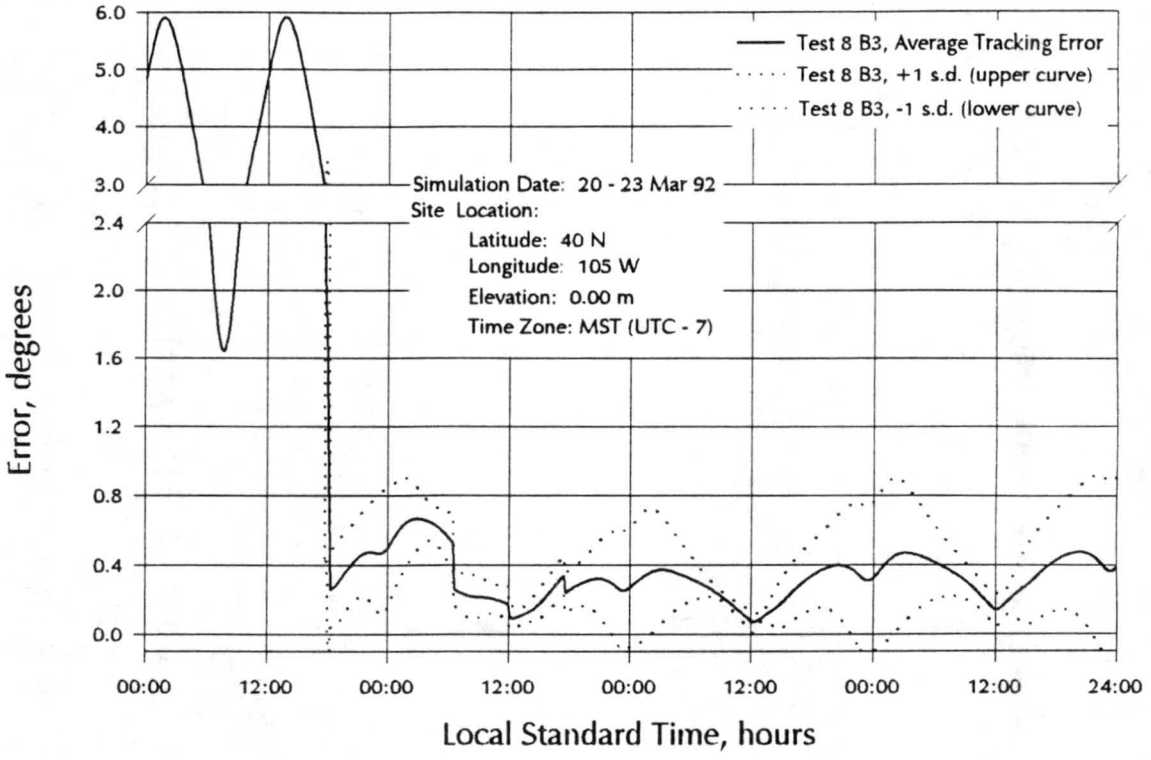

Figure 10: Tracking error for iterative corrections at 6-hour intervals

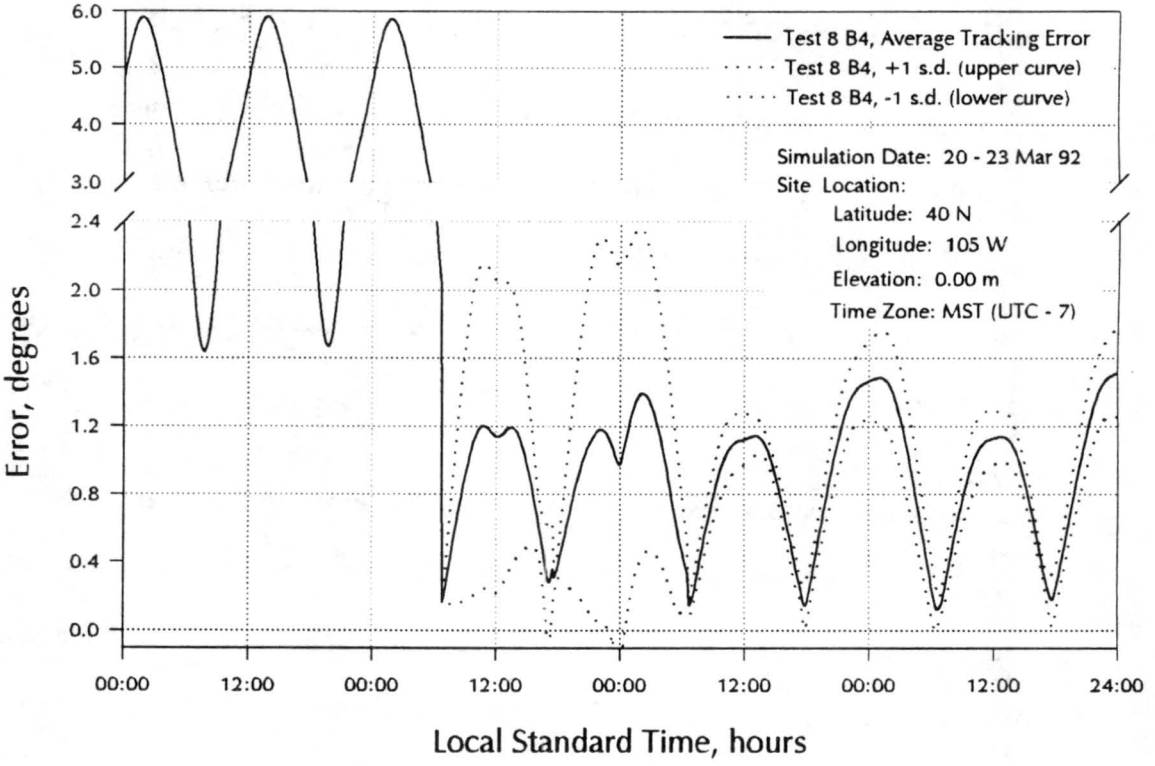

Figure 11: Tracking error for iterative corrections at 12-hour intervals

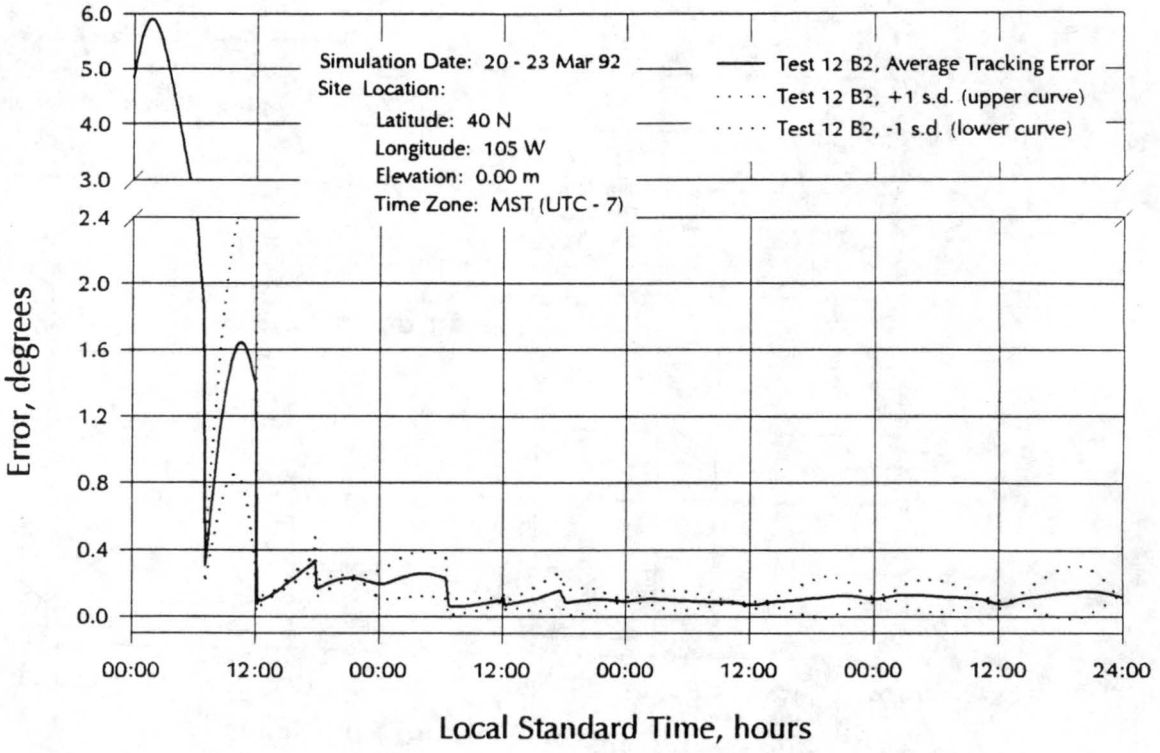

Figure 12: Tracking error for improved iterative correction scheme.

3.3.2 Discussion of Correction Algorithm Test Results

A number of factors were expected to influence the performance of the correction algorithm. These included the initial misalignment of the tracker, errors in the iterative corrections, and the timing of the iterative corrections. The most significant of these were found to be the errors in the iterative corrections and the timing of the iterative corrections.

As would be expected, when the magnitude of the errors in the iterative corrections was reduced, the corrected position of the tracker became more accurate. Also, the minimum and maximum tracking errors appear to have scaled almost linearly with the magnitudes of the iterative correction errors. However, all of the tests in this set used the same

magnitude and orientation of misalignment, so it is unclear whether the scaling would be similar for other misalignments.

The performance of the correction algorithm was strongly sensitive to the timing of the corrections. Multiple corrections made at nearly the same time (*e.g.*, the timing test with 6 corrections at 30-minute intervals) appeared to reduce the effects of random error in the iterative corrections (as evidenced by the small standard deviations), much as replicate measurements reduce the random error in a measurement. However, by itself, this single group of closely-spaced corrections did not provide accurate tracking. Closely-spaced corrections created an $X^T_{lhc} \cdot X_{lhc}$ matrix which was, to some degree, ill-conditioned. Although the SVD technique prevented problems with instability, the $X^T_{lhc} \cdot X_{lhc}$ matrix really didn't contain sufficient information to adequately define the transformation matrix. Thus a good solution to the transformation matrix was not obtained and the tracking error increased rapidly with time.

By spacing iterative corrections over several hours (*e.g.*, the tests with 2-hour and 6-hour intervals between corrections) a good transformation matrix was obtained and tracking error was more stable with time. However, the standard deviation of the tracking error was larger, indicating that the influence of random errors in the iterative corrections was stronger.

When iterative corrections were spaced at 12-hour intervals, extremely poor results were obtained. The tracking error was strongly periodic with an amplitude of about a degree, and did not trend upward. Standard deviations were generally smaller than in the 2-hour and 6-hour tests, but larger than in the 30-minute test. Because a solar day is nearly 24 hours long, the solar position approximately repeats itself every 24 hours. Since

corrections were made at 12 hour intervals, the third correction was essentially a replicate of the first. This appears to have resulted in averaging of the errors in the first and third corrections, leading to some reduction in the standard deviation. At the same time, though, the $X^T_{lhc} \cdot X_{lhc}$ matrix did not contain sufficient information to define the transformation matrix accurately and this led to the cyclic variation in tracking error.

The simulation results suggest that good tracking performance would be achieved if multiple iterative corrections were made in several clusters distributed throughout the day. Using this approach in the simulation, the correction algorithm was capable of controlling the tracking error to within 2σ, σ being the standard deviation associated with the errors in the iterative corrections. Average tracking errors of less than 0.2 degrees were achieved when iterative correction errors were simulated with a standard deviation of 0.153. This performance was maintained for over sixty hours following the final iterative correction.

4. Assessment of Other Sources of Error

4.1 *The Astronomical Algorithm*

The accuracy of the tracker depends in part on the accuracy with which the true solar position is calculated. The algorithm used here to calculate the true solar position was developed by Meeus (1991) from the VSOP87 planetary theory (Bretagnon and Francou, 1988). The algorithm was implemented using a set of C language functions and subroutines written by Sax (1991). Five tests were performed in which the algorithm was used to calculate the true solar position (azimuth and elevation) at ten-minute intervals over a period of twenty-four hours. The test cases were for five distinct days and locations for the year 1992 (Table 5). The results were compared with azimuths and elevations calculated from U. S. Naval Observatory (USNO) data which are accurate to 0.1 minute of arc (0.00167 degrees) (Nautical Almanac Office, U. S. Naval Observatory, 1991). Longitude and altitude were fixed at 105W and 0.00 m respectively.

Table 5: Site data and dates for testing of astronomical algorithm

Test	Date	Latitude
1A	1 Jan 92	40 N
1B	1 Jul 92	40 N
1C	1 Jul 92	80 N
1D	1 Jan 92	80 N
1E	1 Jul 92	0 N

4.1.1 Astronomical Algorithm Test Results

Tests of the algorithm, as implemented on a personal computer with an Intel 80386 processor, showed it to be accurate to better than 0.02 degrees. The comparison showed that the solar positions obtained from the astronomical algorithm deviated by no more than 0.02 degrees from those obtained from the USNO data (Figure 13). Of the five tests performed, these three showed the largest deviations. The remaining two tests showed deviations smaller than 0.007 degrees.

4.1.2 Discussion of Astronomical Algorithm Test Results

Although the maximum tracking errors due to the astronomical algorithm approached 0.02 degrees, the errors ranged from 0.006 degrees to 0.008 degrees over much of the

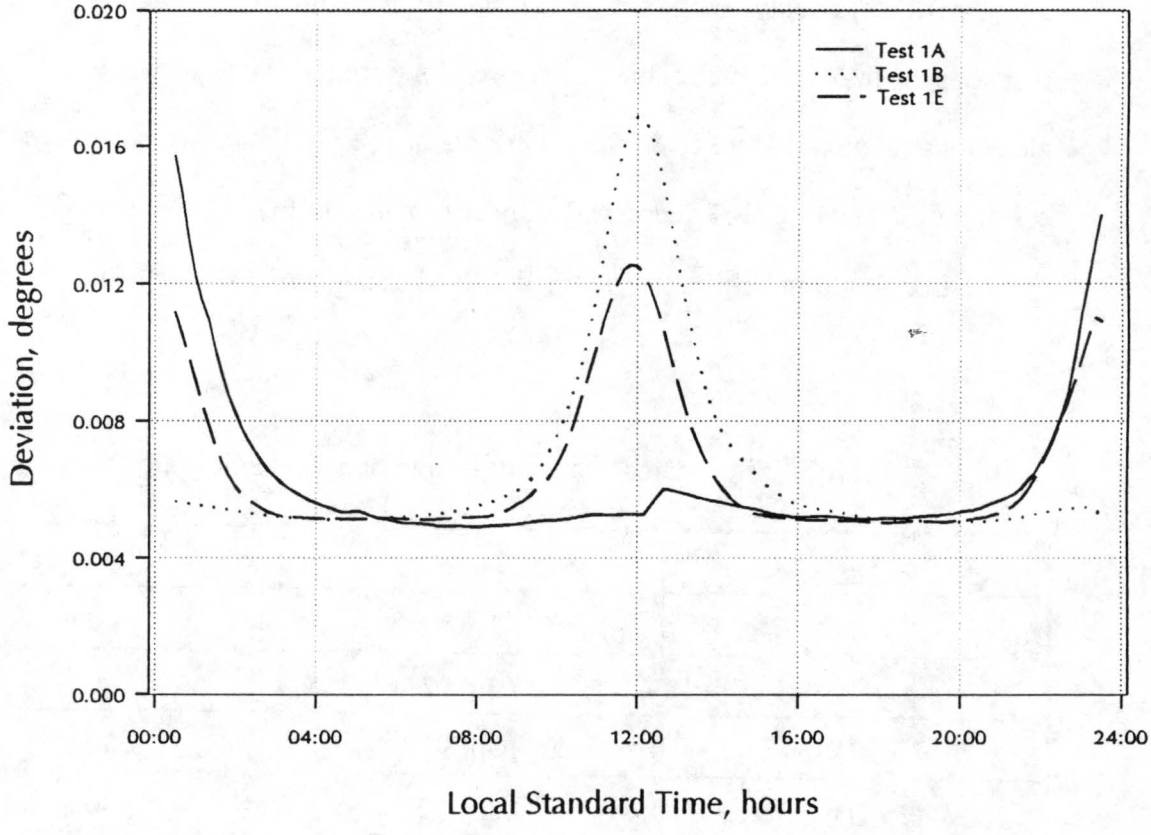

Figure 13: Error in solar position calculated using astronomical algorithm (compared versus positions calculated using U. S. Naval Observatory data).

tests. These errors were small given the fields of view for instruments typically used for atmospheric radiation measurements. For example, at a range of 100 m, an instrument with a 0.5 degree half-angle, circular field of view observes a circular target with a radius of 87.3 cm and an area of 23,943 cm^2. With a tracking error of 0.02 degrees, the observed area is shifted 3.5 cm relative to the target area, resulting in the coverage being shifted by about 611 cm^2 (2.5% of the total target area). With an error of 0.008 degrees, the coverage is shifted only about 244 cm^2 (1% of the total target area).

4.2 *Electromechanical Errors*

Two sources of electromechanical error were noted for the tracking system: servo error and mechanical error. The solar tracker control program measures the servo error by comparing the command position with the position indicated by the optical encoders on the motor shafts. During normal operation of the tracker with a light load in the gimbal (2 - 3 kg), the servo error is typically about 15 encoder counts (0.025 degrees) for each axis. An estimate of the mechanical error is available from manufacturer's literature for the optical mount (Aerotech, 1991). The accuracy for each axis is specified as 0.05 degrees.

5. System Testing and Performance

5.1 *Field Testing of the System*

The previous sections isolated and examined three sources of tracking error: misalignment, the astronomical algorithm and the electromechanical system. The tracking error correction algorithm was tested only for its ability to correct for misalignment; however, during actual operation of the tracker, all three sources of error are present. It was unclear how the tracking error correction algorithm would perform when all three sources of error were present. To evaluate this, a field test was performed on the complete system.

For this test, the tracker was set up in the field with an intentional misalignment, a series of iterative corrections were made, then the tracking error was measured over a two-day period. The tracker was mounted on a sturdy aluminum table and the table was rotated about its vertical axis to an azimuth error of about +1.5 degrees. Then the table was tilted approximately 1.2 degrees (downward to the west). To improve the resolution of the subsequent iterative corrections and measurements, the tracker was zeroed to a point marked on a wall about 30 m south of the tracker.

Iterative corrections were made on the first and fourth days of the test. The timing for the iterative corrections was based on a scheme developed from the results of the sensitivity testing described above. Iterative corrections were made in clusters of three, and three clusters were made each day. The clusters were separated by about three hours (four

hours on the fourth day) and individual corrections within each cluster were separated by about five minutes. The tracker was operated in mirror mode, so the solar image was projected to the zero point on the wall south of the tracker. Iterative corrections were made so that the solar image was centered on the zero point.

On the fifth and sixth day of the test, no corrections were made, and the tracking error was measured at approximately half-hour intervals. The distance from the center of the solar image to the zero point was measured and converted to an angular error. The precision with which this measurement could be made was estimated as 2 cm, which resulted in 0.04 degrees of uncertainty.

5.1.1 Results of System Field Testing

Testing of the solar tracker in the field showed tracking errors ranging from 0.06 degrees to 0.18 degrees over a two-day period following the final iterative correction (Figure 14). The tracking error appeared to vary somewhat periodically, much as occurred in the simulations. Averaged over all measurements, the tracking error was 0.11 degrees.

5.1.2 Discussion of System Field Test Results

The performance of the tracker when tested in the field was similar to the performance predicted by the tests with the simulation. In the simulation test which used the optimized scheme for iterative corrections, tracking errors were less than 0.2 degrees. For this field test, the average tracking error was 0.11 +/- 0.04 degrees with a maximum error of 0.18 +/- 0.04 degrees. How do these tracking errors compare with the errors in the iterative corrections? When projected to the zero point at a range of about 30 m, the image of the solar disk was a fairly well-defined bright circle with a diameter of

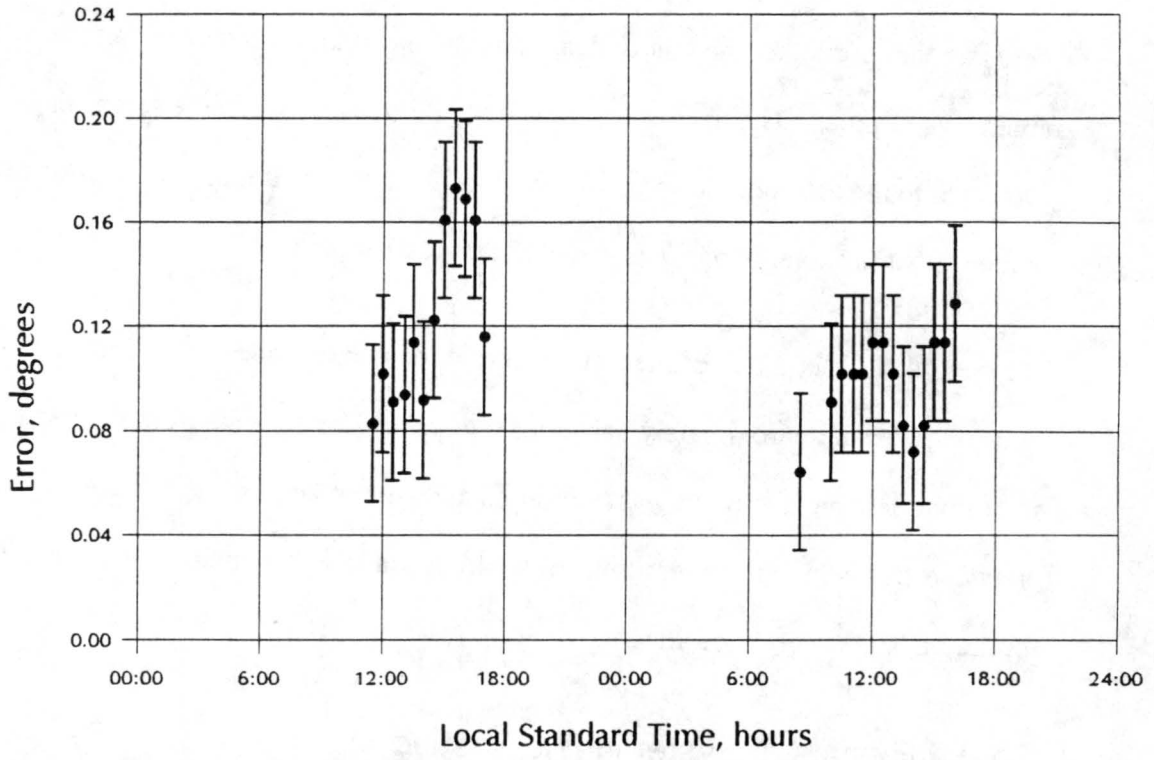

Figure 14: Tracking error for field testing with improved iterative correction scheme

approximately 35 cm. The target area was ruled with concentric circles at 15 cm increments of radius. When iterative corrections were made, the position of the solar disk could typically be adjusted so that it was misaligned by no more than about half the spacing between the circles on the target, or about 7.5 cm. This is equal to an uncertainty of about 0.14 degrees in the iterative corrections. Thus, in this field testing, the maximum tracking error was slightly larger than the uncertainty in the iterative corrections, just as was observed in the tests with the simulation. The orientation of misalignment was similar to axis B used in the simulation tests, with a magnitude on the order of 5 degrees.

6. Methods Used in Mirror Scatter Testing

6.1 *Mirror Scattering Effects*

Scattering from optical elements such as mirrors and lenses in an instrument may contaminate the signal produced by the instrument. If light from a non-target object (an object outside the instrument's field of view) is incident on such an element, that light may be scattered into the instruments's field of view and contribute to the measured flux, even though the object lies outside the field of view. If the target object is bright, while the non-target objects are dim, the contamination is likely insignificant. An example would be making radiometric observations of the sun through a clear sky. The signal due to the sun is much stronger than the signal due to the scattering of diffuse skylight into the radiometer's field of view. The contamination may be significant if the situation is reversed, *i.e.*, observing a dim target like diffuse skylight in the presence of a bright non-target object like the sun. If the direct solar beam strikes an element in the optical path of the instrument and if even a small fraction of the beam is scattered into the field of view, the scattered light may significantly contaminate the measurement.

In the solar tracking system, measurements may be made in either direct mode or mirror mode. In mirror mode, contamination may result from scattering from the mirror surface. It may not be possible to shade the mirror adequately to prevent this contamination, especially as the position of the sun changes with time. Then it is necessary to determine whether the contamination is significant compared to the signal being measured. If the contamination is significant, it's important to know if the contamination is predictable or

if it is possible to specify a mirror with properties that adequately reduce the contamination.

The primary concern, then, is the case when a mirror is used in the solar tracking system with an instrument which is observing diffuse skylight. In that case, the total signal produced by the instrument can be partitioned into signals from three distinct sources:

- **Target reflection**
  the light exiting the target which is specularly reflected by the mirror into the instrument,
- **Solar scattering**
  the light from the direct solar beam which is scattered by the mirror into the instrument, and
- **Background scattering**
  the light from other miscellaneous sources which is scattered by the mirror into the instrument.

The first item in the list is the desired signal. The other two items are contaminants. Both of these contaminants depend on the scattering properties of the mirror along with the intensity and spatial distribution of the undesirable light sources which are incident on the mirror. The second item may be predicted if the scattering properties of the mirror are known along with the irradiance and direction of the direct solar beam. The third item appears unpredictable due to the complexity and variability of the incident sources.

6.2 *Mirror Scattering Properties*

The scattering properties of a surface can be described in terms of the bidirectional reflectance distribution function (BRDF) (Stover, 1990; Nicodemus *et al.*, 1977). The BRDF relates the radiance scattered from a point on a surface to the irradiance incident on that point. If the scattering properties of the surface are uniform and isotropic, the BRDF can be expressed as (Nicodemus *et al.*, 1977):

$$f_r(\theta_i,\phi_i,\theta_s,\phi_s) = dL_r(\theta_i,\phi_i,\theta_s,\phi_s;E_i) / dE_i(\theta_i,\phi_i) \tag{14}$$

or, alternately, in terms of the incident radiance:

$$f_r(\theta_i,\phi_i,\theta_s,\phi_s) = dL_r(\theta_i,\phi_i,\theta_s,\phi_s;E_i) / (L_i(\theta_i,\phi_i)\cos(\theta_i)d\omega_i) \tag{15}$$

where f_r is the BRDF, dL_r is the scattered radiance, E_i is the incident irradiance, L_i is the incident radiance, and $d\omega_i$ is the infinitesimal solid angle through which L_i is incident. The angles (θ_i, ϕ_i, θ_s, ϕ_s), which define the directions of the incident and reflected radiances, are defined as shown in Figure 15.

The BRDF is closely related to the topography of the reflecting surface. Provided the surface is a clean, optically smooth, front-surface reflector, the BRDF can be related to the power spectral density function (PSD) of the surface profile by using the Rayleigh-Rice vector perturbation theory (Stover, 1990). The PSD gives the square of

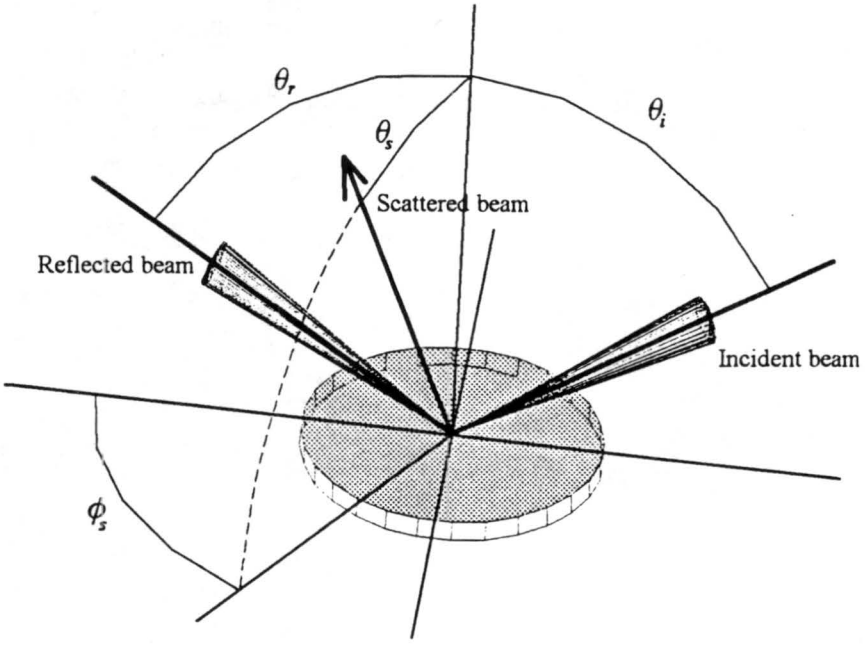

Figure 15: Scattering geometry

the surface roughness height per unit spatial frequency. The BRDF and PSD are related by:

$$f_r(\theta_i,\phi_i,\theta_s,\phi_s)=\frac{16\pi^2}{\lambda^4}\cos(\theta_i)\cos(\theta_s)Q(\theta_i,\theta_s,\phi_s)S(f_x,f_y) \tag{16}$$

where λ is the wavelength of the incident light, Q is a polarization factor which relates the polarization states of the incident and scattered beams, and S is the PSD, which is a function of the spatial frequencies f_x and f_y. Thus, given a particular surface profile (*i.e.*, a particular PSD), (16) allows the BRDF to be expressed as a function of wavelength, polarization and incident angle, provided the conditions of Rayleigh-Rice theory are met. If the incident beam is unpolarized, and the receiver is insensitive to polarization, Q is given by:

$$Q=\frac{1}{2}\left[Q_{ss}+Q_{sp}+Q_{ps}+Q_{pp}\right] \tag{17}$$

where Q_{ss}, Q_{sp}, Q_{ps}, and Q_{pp} represent the various combinations of incident and detected polarization states and are approximated for good reflectors by (Stover, 1990):

$$Q_{ss}=\cos^2(\phi_s) \tag{17a}$$

$$Q_{sp}=\left(\frac{\sin(\phi_s)}{\cos(\theta_s)}\right)^2 \tag{17b}$$

$$Q_{sp}=\left(\frac{\sin(\phi_s)}{\cos(\theta_i)}\right)^2 \tag{17c}$$

$$Q_{pp}=\left(\frac{\cos(\phi_s)-\sin(\theta_i)\sin(\theta_s)}{\cos(\theta_i)\cos(\theta_s)}\right)^2 \tag{17d}$$

The spatial frequencies f_x and f_y are derived from the hemispherical grating equations for diffraction and are defined by:

$$f_x = \frac{\sin(\theta_s)\cos(\phi_s) - \sin(\theta_i)}{\lambda} \tag{18a}$$

$$f_y = \frac{\sin(\theta_s)\sin(\phi_s)}{\lambda} \tag{18b}$$

Assuming the surface is isotropic, f_x and f_y can be reduced to a single frequency, f_{iso}, where:

$$f_{iso} = (f_x^2 + f_y^2)^{1/2} \tag{18c}$$

6.3 *Field Tests of Mirror Scattering*

To assess the significance of the scattering terms, a series of tests was performed which allowed the individual components of the mirror-mode measurement (target reflection, solar scattering and background scattering) to be calculated and compared with the direct-mode measurement. In addition, the solar scattering was used to calculate the BRDF and PSD for the mirror. A sunphotometer was used to make measurements of the solar beam and of diffuse skylight both directly (*i.e.*, with the sunphotometer pointed at the sky) and through the mirror (with the sunphotometer pointed at the mirror and the mirror positioned to reflect skylight into the sunphotometer). Specifications for the sunphotometer and mirror are shown in Table 6. Over the course of three days, the test was repeated three times for each of two wavelengths (Table 7).

The BRDF varies with the incident and scattering directions, so data had to be collected for a range of scattering geometries. Note from Figure 15 that the coordinate system for the scattering geometry is defined by the normal to the mirror surface and the azimuth direction of the reflected beam. Since solar scattering was used for the BRDF calculation, the direction of the reflected solar beam defined the azimuthal coordinates.

Then the scattering geometry was varied by changing the position of the diffuse target. With the solar tracker, the position of the diffuse target can be specified by an offset from the current solar position. The tracker expresses offsets in units of time. To obtain the offset position, the tracker software calculates the solar position at the current local time

Table 6: Specifications for the sunphotometer and mirror

Sunphotometer:		
	Manufacturer:	University of Arizona
	Telescope:	Field of view 2 degrees, full angle Entrance aperture 0.75 inches
	Detector:	Photodiode, EG&G model UV-444B Temperature stabilized, photovoltaic operation
	Filters:	Ten narrow-band three-cavity interference filters Bandpasses between 7 and 15 nm, FWHM
Mirror:		
	Design:	8-inch, aluminized, front-surface with a protective coating.
	Flatness:	Unspecified

Table 7: Parameters for the mirror scattering tests

Test	Date & Time	Wavelength, nm	Offsets relative to sun, minutes
A	1 Oct. 97, am	440.9	+25 to +180
B	5 Oct. 97, pm	440.9	-35 to -180
C	6 Oct. 97, pm	440.9	-35 to -180
D	1 Oct. 97, am	779.0	+25 to +180
E	5 Oct. 97, pm	779.0	-35 to -180
F	6 Oct. 97, pm	779.0	-35 to -180

plus the specified offset. This position becomes the target position for the tracker. For these measurements, the offsets ranged in magnitude from 25 minutes to 180 minutes, giving angular offsets (relative to the solar position) ranging approximately from 7 degrees to 45 degrees. Smaller offsets could not be used because of problems with scattering of the solar beam by the objective lens of the sunphotometer. These angular offset positions were later used to calculate the scattering geometry.

In order for the measurements at each offset to be useful, the target observed in the direct measurement should be the same as the target observed in the mirror measurement (implying that, ideally, the direct and mirror measurements should be made simultaneously and at precisely the same target). However, since the sunphotometer had to be repositioned to switch from direct mode to mirror mode, simultaneous direct and mirror measurements were not possible. Therefore, it was necessary to make sequential direct and mirror measurements at each offset and to minimize the elapsed time between measurements. Also, measurements were confined to days with minimal cloudiness, so as to minimize the spatial and temporal variability of the illumination from the sky.

Two mounting positions were set up for the sunphotometer. For direct measurements, a bracket was attached to the back of the gimbal's optics ring. This allowed the sunphotometer to be mounted on the gimbal, above and behind the mirror so as not to interfere with the gimbal's rotation. For mirror measurements, an instrument stand was clamped to the tracker table at a point approximately south of the tracker. The instrument stand was positioned such that, when the sunphotometer was mounted on the stand, the sunphotometer was approximately aligned so that light from the tracker's target would be reflected into it's aperture.

Prior to taking measurements, the mirror was mounted in the gimbal and the tracker was started following the procedures described in Wood *et al.* (1996). For direct measurements, the sunphotometer was first mounted on its bracket on the gimbal. An iterative correction was made so that the sunphotometer was pointed directly at the sun, then the direct measurements were made. Next the sunphotometer was moved from the gimbal to its instrument stand. The tracker was switched to mirror mode, any offset was removed, and, if necessary, an iterative correction was applied so that the reflected solar beam was incident on the sunphotometer. Then the mirror measurements were made. Next the sunphotometer was returned to its bracket on the gimbal, realigned and the remaining direct measurements were made.

The data set taken for each particular offset angle consisted of seven data points:

- **direct-solar**
  sunphotometer pointed directly at the sun, at solar zenith angle $\theta_{sol,1}$
- **direct-offset**
  sunphotometer pointed directly at a patch of diffuse skylight at offset angle α
- **mirror-solar**
  sunphotometer pointed at the mirror, viewing the sun, at solar zenith angle $\theta_{sol,2}$
- **mirror-offset-sun**
  sunphotometer pointed at the mirror, viewing a patch of diffuse skylight at offset angle α, with the solar beam incident on the mirror
- **mirror-offset-nosun**
  sunphotometer pointed at the mirror, viewing a patch of diffuse skylight at offset angle α, with the solar beam obscured from the mirror
- **direct-solar**
  sunphotometer pointed directly at the sun, at solar zenith angle $\theta_{sol,3}$
- **direct-offset**
  sunphotometer pointed directly at a patch of diffuse skylight at offset angle α

The direct-solar and direct-offset measurements were repeated in order to bracket the variation in the signals for the direct solar beam and the diffuse target. The elapsed time from the beginning to end of a single set of measurements was approximately ten minutes. The local standard time, the sunphotometer gain (typically in millivolts of output signal per microamp or nanoamp of photodiode current), and the sunphotometer output (in millivolts) were recorded at each measurement. Since the PSD should be independent of the wavelength at which measurements are made (the PSD describes the physical properties of the mirror), measurements were taken in two bands, one centered at 440.9 nm and the other 779.0 nm.

For each measurement, geometric calculations were performed to obtain the offset angle (for offset measurements), the solar zenith angle in local horizontal coordinates, the scattering angles, and the spatial frequency coordinates f_x and f_y. Also, the sunphotometer output in millivolts was converted to photodiode current in nanoamps, based on the gain recorded at the measurement.

As noted above, when the mirror is used to observe diffuse skylight, the radiance exiting the mirror can be considered to be due to three terms: target reflection, solar scattering and background scattering. Then the signal from an instrument observing that radiance can be written as the sum of the signals due to each term:

$$\begin{aligned} i_{mirror-offset} &= i_{spec} + i_{scat,solar} + i_{scat,background} \\ &= R_{spec} i_{direct-offset} + i_{scat,solar} + i_{scat,background} \end{aligned} \tag{19}$$

where $i_{mirror\text{-}offset}$ is the total signal output by the instrument for a mirror-offset measurement, i_{spec} is the signal due to the specularly reflected target ($= R_{spec} i_{direct\text{-}offset}$, where R_{spec} is the specular reflectance of the mirror and $i_{direct\text{-}offset}$ is a measured

direct-offset signal), $i_{scat,solar}$ is the signal due to scattering of the direct solar beam, and $i_{scat,background}$ is the signal due to scattering of other light incident on the mirror.

The data were then analyzed to evaluate the individual terms in (19). First, the specular reflectance of the mirror was found by calculating the ratio of the mirror-solar measurement to the direct-solar measurement:

$$R_{spec} = \frac{i_{mirror-solar}}{i_{direct-solar}} \tag{20}$$

Since a direct-solar measurement was not made simultaneously with the mirror-solar measurement, the value for $i_{direct-solar}$ was interpolated from the initial and final direct-solar measurements. This was done by assuming a Beer's Law dependence on zenith angle and interpolating to the solar zenith angle at the time of the mirror-solar measurement. Then the ratio was calculated, giving R_{spec} as a function of incident angle relative to the mirror normal for each of the two wavelengths. The dependence on incident angle was weak, so an arithmetic mean value for each wavelength was used in subsequent calculations.

Next, $i_{direct-offset}$ was determined. Since neither of the two direct-offset measurements were simultaneous with the mirror-offset measurement, the direct-offset measurements were interpolated to the position of the mirror-offset measurement. In this case, an arithmetic mean of the initial and final direct-offset measurements was used.

Next, $i_{scat,solar}$ was expressed as the difference between the measurements mirror-offset-sun and mirror-offset-nosun. These two measurements were typically made within a few seconds of each other and were treated as being simultaneous.

Finally, $i_{scat,background}$ was determined from:

$$i_{scat,background} = i_{mirror-offset} - R_{spec} i_{direct-offset} - i_{scat,solar} \tag{21}$$

For each replicate set of measurements, a BRDF was then calculated using (14), with dL_r given by $i_{scat,solar}/(\Omega \cos(\theta_s))$, where Ω is the field of view of the sunphotometer in steradians, and dE_i given by $i_{direct-solar}\cos(\theta_i)$. Each BRDF was then converted to a PSD using (16) - (18). The resulting PSD's were plotted versus f_{iso} for comparison with each other.

For many optical surfaces the PSD very nearly follows an inverse power law (Stover, 1990). In such a case, if we assume the mirror scattering properties are isotropic, the PSD can be expressed as:

$$S(f_x) = \frac{K_n}{f_x^n} \tag{22}$$

where K_n and n are constants.

Once the PSD is known, it can be used to predict the BRDF at other wavelengths, incident angles and reflected angles, provided the mirror scatters according to Rayleigh-Rice theory. Given θ_i, θ_s, ϕ_s, and λ, then f_x, f_y, and Q can be calculated. Using f_x and f_y, a value of $S(f_x, f_y)$ can be interpolated from the data, or, if the spatial frequencies are outside the range of the data, the inverse power law can be used to extrapolate $S(f_x, f_y)$ to the required spatial frequencies. Once $S(f_x, f_y)$ is known, the BRDF can be calculated using (16).

Given the BRDF and an incident irradiance E_0, the scattered radiance L_r can be calculated. Rearranging (15) to solve for the reflected radiance gives:

$$L_r(\theta_s,\phi_s) = \int_{\Omega_i} f_r(\theta_i,\phi_i,\theta_s,\phi_s) L_i(\theta_i,\phi_i)\cos(\theta_i)\, d\omega_i \tag{23}$$

Equation 23 indicates that, for a non-specular reflector, any incident light, from a direction in which f_r is not zero, contributes to the scattered radiance. If the incident irradiance is from the sun, the direct solar beam may be approximated using the Dirac delta function (Liou, 1980):

$$L_i(\theta_i,\phi_i) = E_0 \delta(\theta - \theta_i)\delta(\phi - \phi_i) \tag{24}$$

where E_0 is the solar irradiance perpendicular to the direct beam. This approximation allows (24) to be evaluated as:

$$L_r(\theta_s,\phi_s) = E_0 \cos(\theta_0) f_r(\theta_0,\phi_i,\theta_s,\phi_s) \tag{25}$$

If the incident radiance is from a more general source, such as diffuse skylight, the integral (23) will most likely have to be solved using numerical techniques.

7. Mirror Scattering Test Results

The results of the mirror scattering tests are cumbersome to present graphically, because, at a given wavelength, the BRDF depends on four variables: θ_i, ϕ_i, θ_s, and ϕ_s (the zenith and azimuth angles, relative to the mirror normal, for both the incident and scattered beams). Normally, tests would be performed with the direction of the incident beam fixed and with measurements made along a constant ϕ_s so that only one independent variable remains. However, in these tests, the direction of the incident beam is not fixed, nor is ϕ_s, due to the changing position of the sun and the mirror normal. The dependencies can be simplified somewhat by assuming that the scattering properties of the mirror are isotropic, so that the BRDF is independent of incident azimuth angle but still dependent on θ_i, θ_s, and ϕ_s. Still, these parameters vary considerably over even a single set of measurements. So, to simplify further, the raw measurements of the signals for the specular reflection, solar scatter and background scatter are presented only as functions of offset angle.

At both wavelengths, solar scattering and background scattering make measurable contributions to the desired signal. After the measurements were decomposed per (19), the target reflection (i_{spec}), the solar scatter ($i_{scat,solar}$) and the background scatter ($i_{scat,background}$) were plotted versus offset angle (Figures 16 and 17). In general, i_{spec} decreases with increasing offset angle. In tests A and D, i_{spec} initially decreases, then increases with increasing offset angle. Values for $i_{scat,background}$ vary only slightly with offset angle. Values for $i_{scat,solar}$ are higher at small offset angles, then decrease with

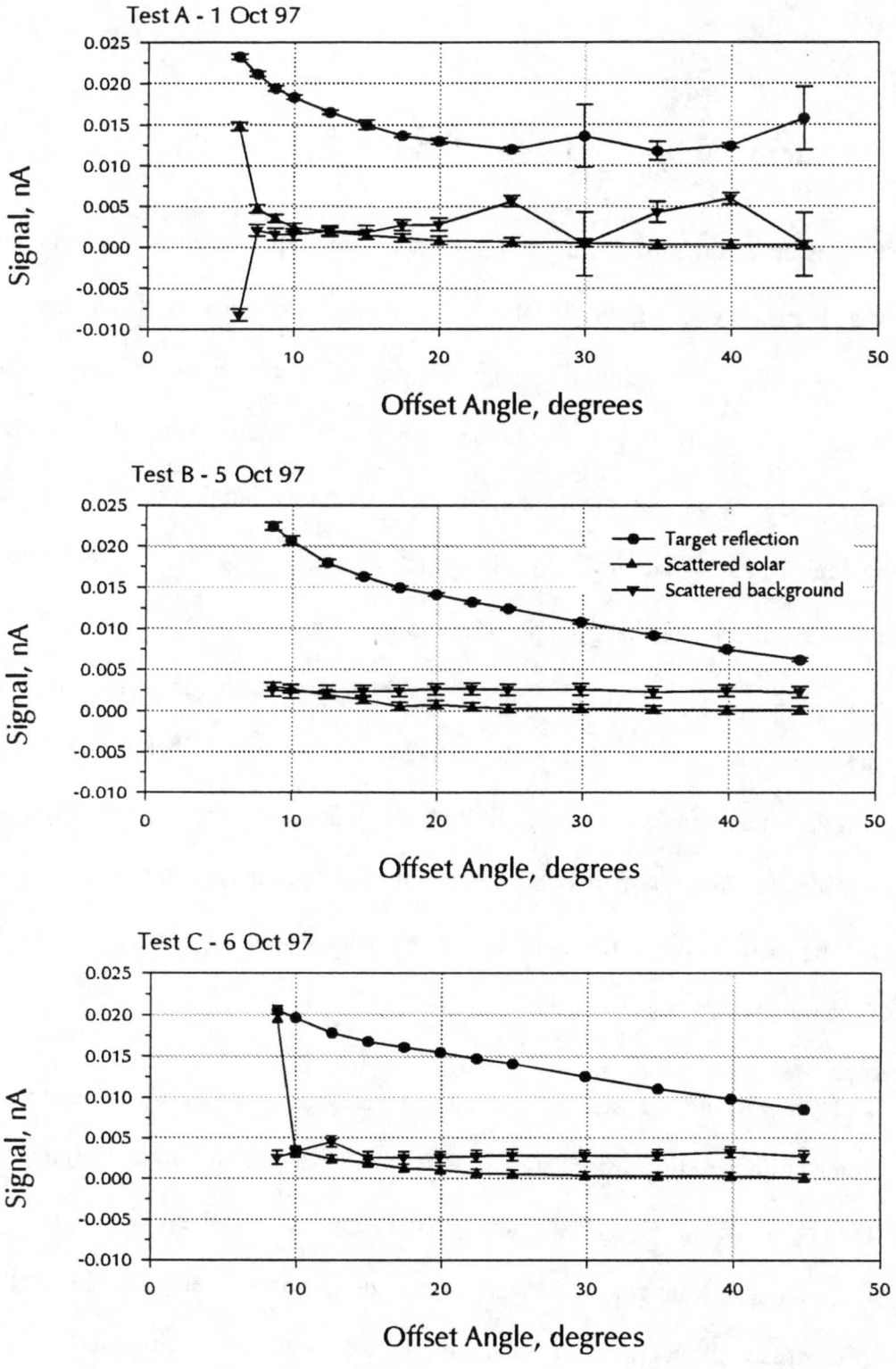

Figure 16: Target reflection, solar scattering and background scattering as a function of offset angle for for $\lambda = 440.9$ nm

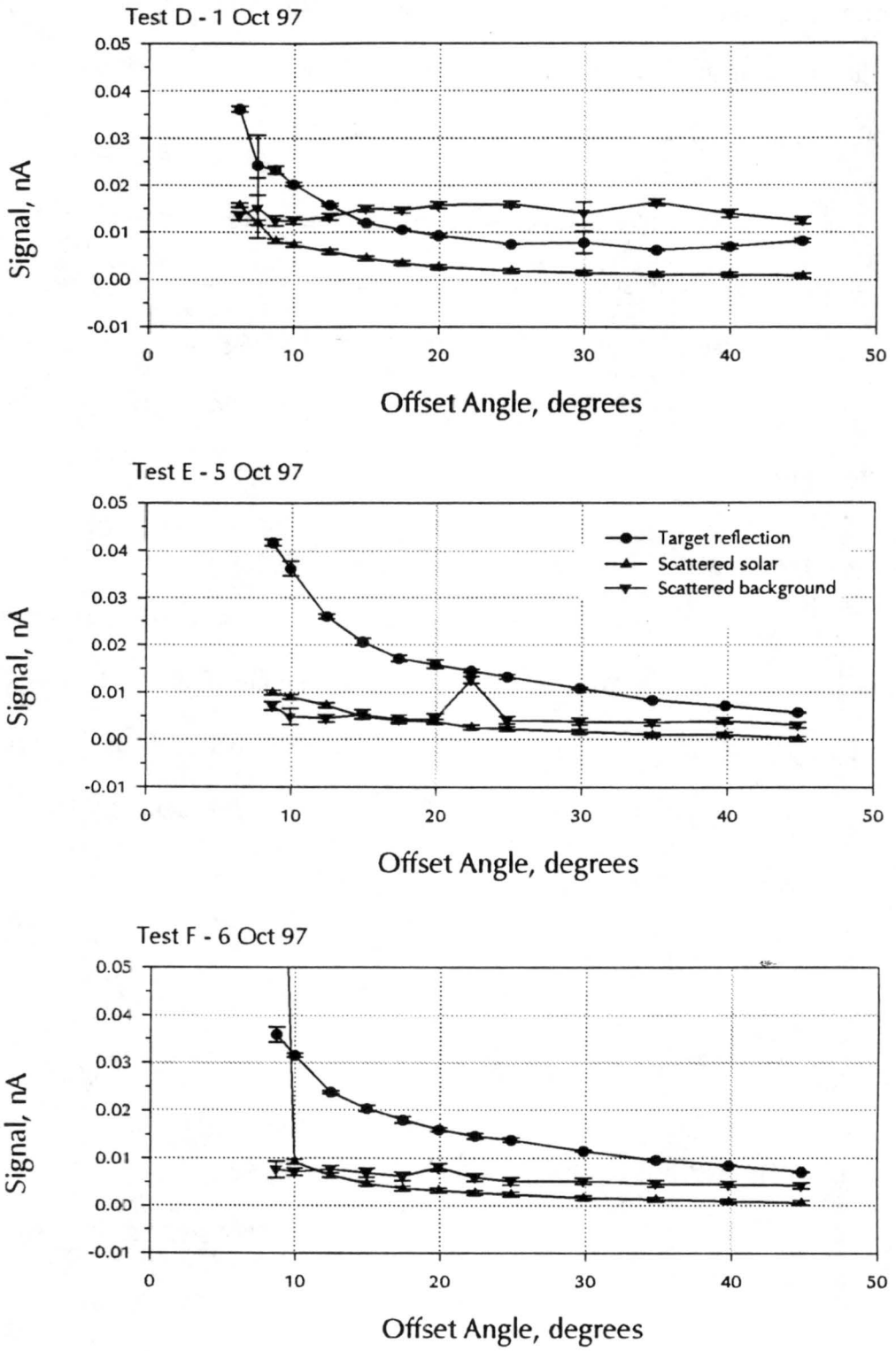

Figure 17: Target reflection, solar scattering and background scattering as a function of offset angle for for λ = 779.0 nm

increasing offset angle. In some cases, at the smallest offset angles, unusually high values of solar scatter are indicated. This appears to be a result of scattering of the reflected solar beam by the objective lens of the sunphotometer.

The relative magnitudes of the solar and background scattering components (as a percent of the total mirror-offset signal) were also calculated (Figures 18 and 19). At 440.9 nm, the scattering terms range from 20% to 40% of the total signal. At 779.0 nm, the scattering terms are even more significant, ranging from 20% to as high as 70% of the total signal.

The solar scatter data were reduced to BRDF's for each test. Provided that the surface can be described in terms of the grating equations (this is somewhat less restrictive than the full requirements of Rayleigh-Rice theory) then each BRDF can be scaled to the same value for θ_i (Stover, 1990). Provided the surface is isotropic, each BRDF can be further scaled to the same value of ϕ_s, leaving θ_s as the only independent variable. For the PSD of an isotropic mirror,

$$S(f_x, f_y) = S(f_x', f_y') \tag{26}$$

provided that $[f_x^2 + f_y^2]^{1/2} = [(f_x')^2 + (f_y')^2]^{1/2}$.

Solving (15) for the PSD and substituting into (26) gives:

$$f_r(\theta_i', \theta_s', \phi_s') = f_r(\theta_i, \theta_s, \phi_s) \frac{\cos(\theta_i')\cos(\theta_s') Q(\theta_i', \theta_s', \phi_s')}{\cos(\theta_i)\cos(\theta_s) Q(\theta_i, \theta_s, \phi_s)} \tag{27}$$

Assuming that we want to find the BRDF for normal incidence, we choose the common values for the directional angles to be $\theta_i' = \phi_i' = \phi_s' = 0$.

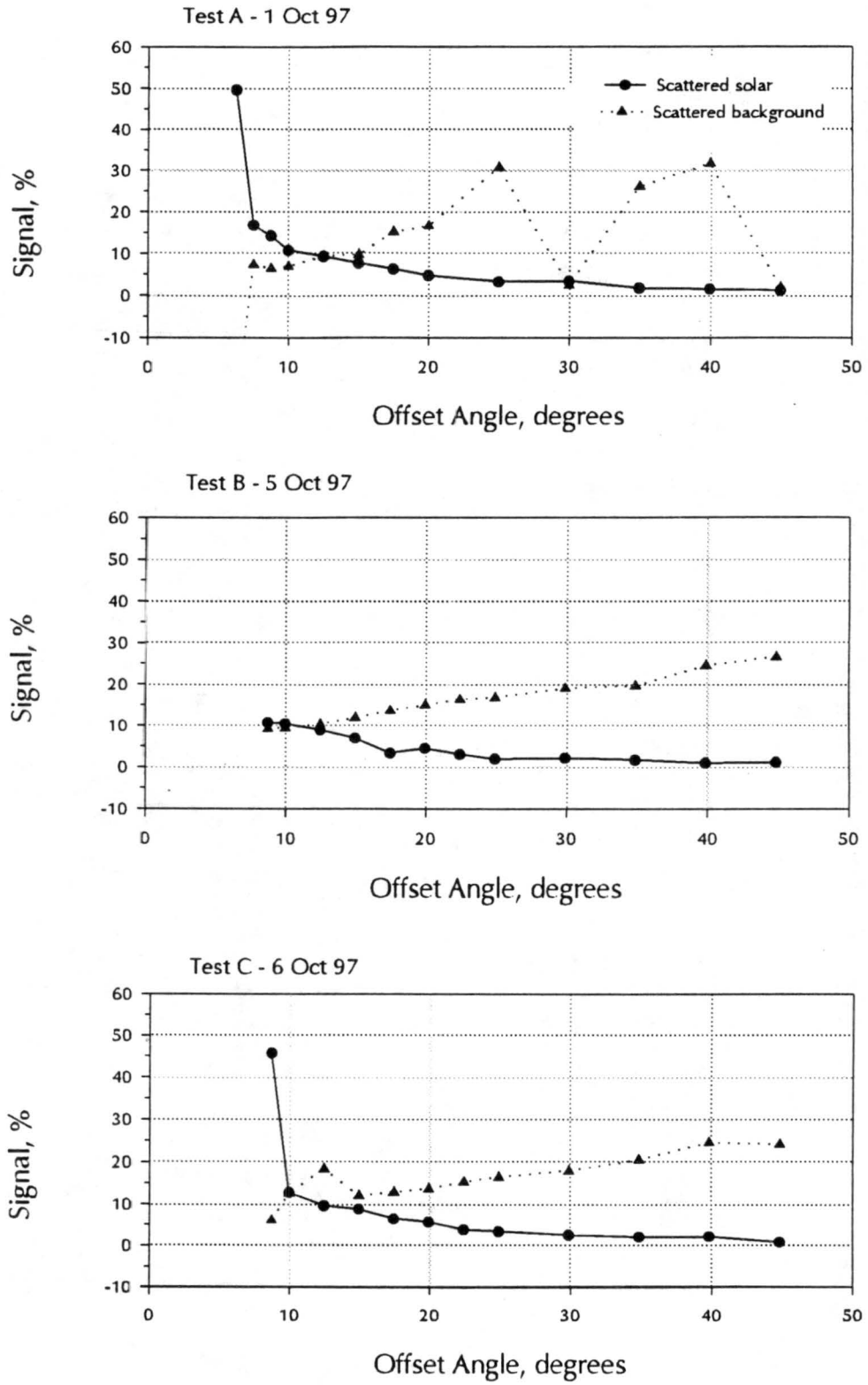

Figure 18: Magnitudes of solar scattering and background scattering, as % relative to the total mirror-offset signal, as a function of offset angle, for $\lambda = 440.9$ nm

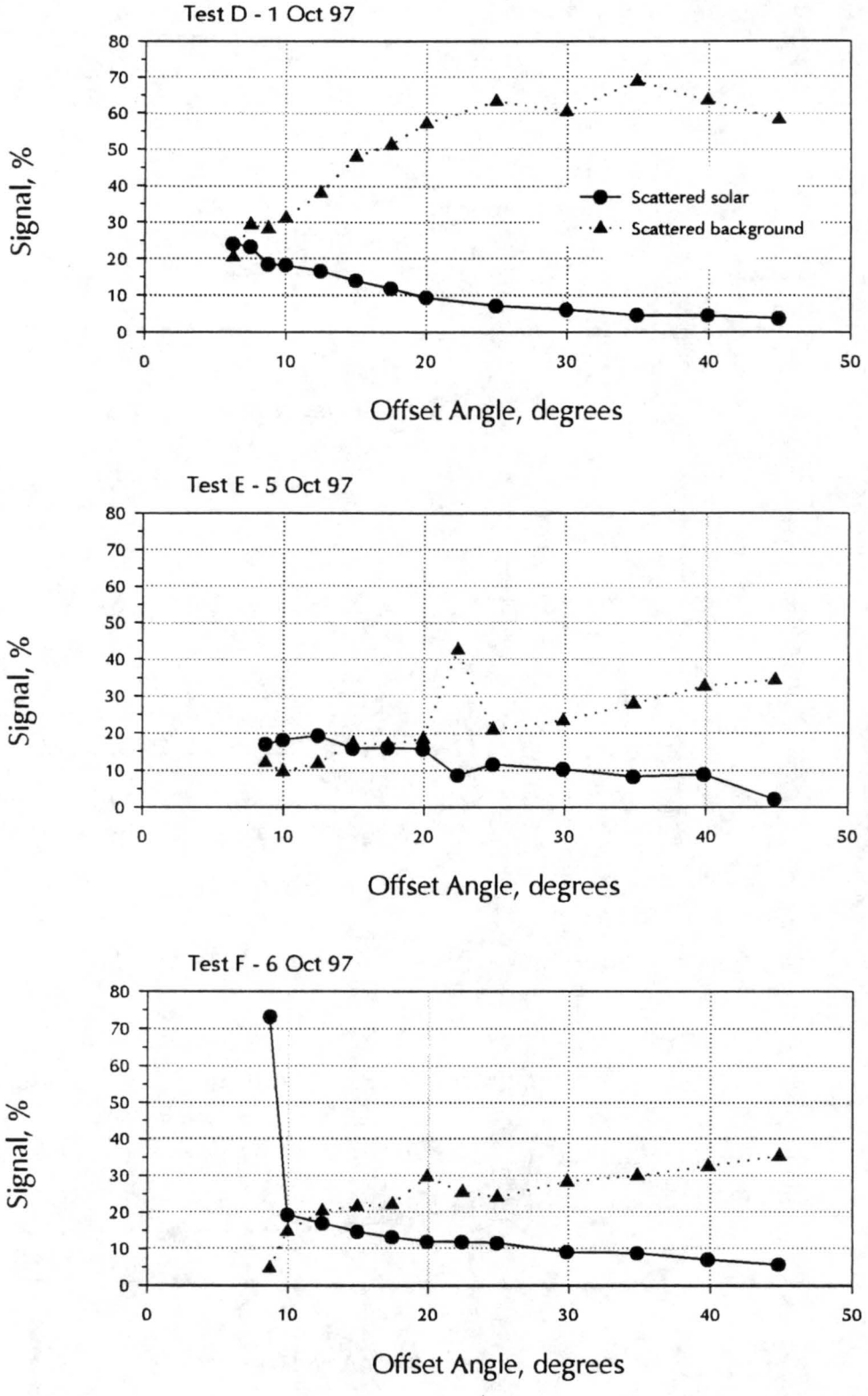

Figure 19: Magnitudes of solar scattering and background scattering, as % relative to the total mirror-offset signal, as a function of offset angle, for $\lambda = 779.0$ nm

Since $\phi_s' = 0$, then from (18b) $f_y' = 0$ and:

$$f_x' = [f_x^2 + f_y^2]^{1/2} \tag{28}$$

θ_s' is found from (18a) as:

$$\theta_s' = \sin^{-1}(\lambda f_x') \tag{29}$$

Then

$$f_r(0,\theta_s',0) = f_r(\theta_i,\theta_s,\phi_s)\frac{\cos(\theta_s')Q(0,\theta_s',0)}{\cos(\theta_i)\cos(\theta_s)Q(\theta_i,\theta_s,\phi_s)} \tag{30}$$

allowing the BRDF to be plotted solely as a function of θ_s' (Figures 20 and 21).

The BRDF values are generally higher at small scattering angles and decay to lower values at large scattering angles. The measurements appear reasonably repeatable among

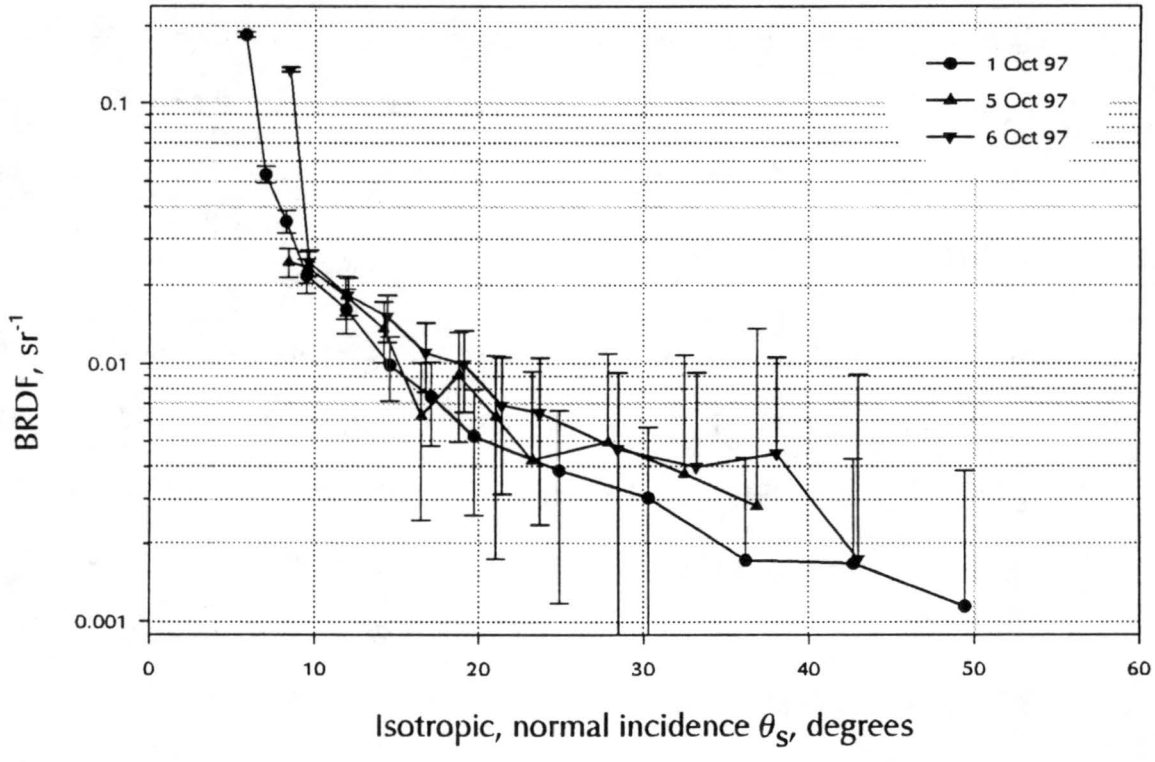

Figure 20: Scaled BRDF for normal incidence, plane of incidence measurement, $\lambda = 440.9$ nm

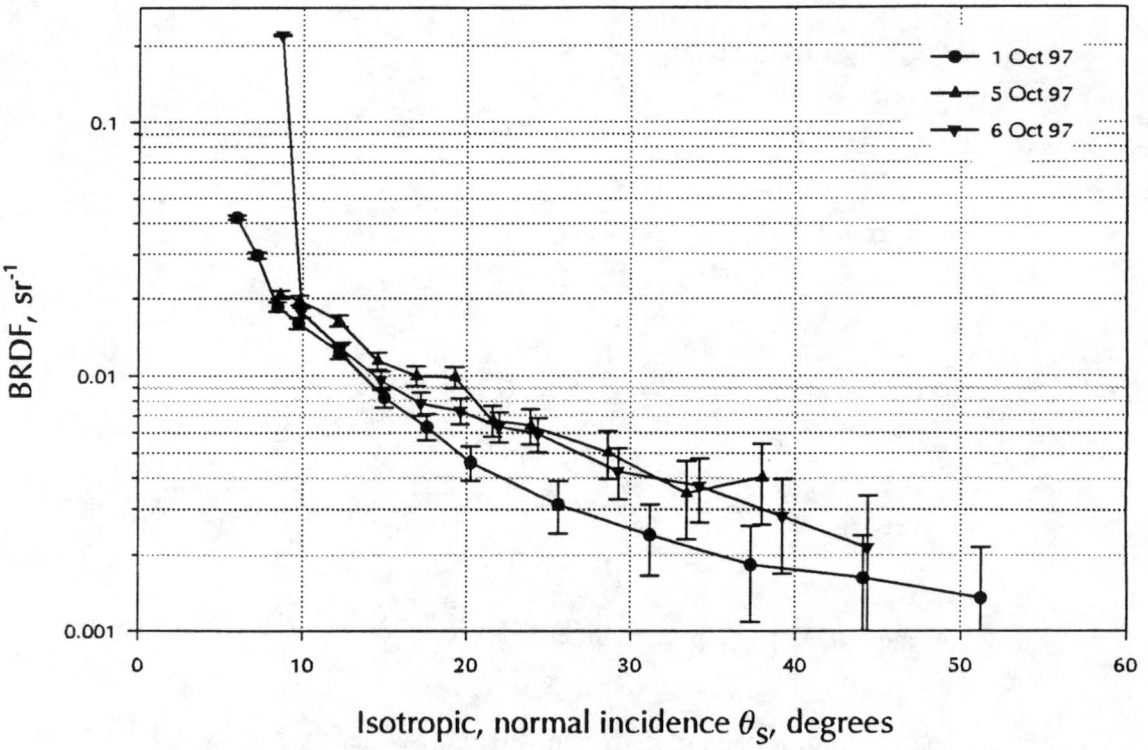

Figure 21: Scaled BRDF for normal incidence, plane of incidence measurement, $\lambda = 779.0$ nm

the three replicate tests performed at each wavelength. At small scattering angles, the BRDF's for $\lambda = 440.9$ appear to be somewhat larger than those for $\lambda = 779.0$. At larger scattering angles, the differences seem less significant. Again, there are some anomalous results at the smallest scattering angles.

Power spectral density data were also derived from the measurements and plotted versus f_{iso} (Figures 22 and 23). Following (22), nonlinear regression was performed on the data (excluding the PSD values for the anomalous solar scatter values already noted) so that values for n and K_n could be determined (Table 8). The standard errors for each parameter and the correlation coefficient for the regression are also shown in the table. The figures and linear regression results show that the PSD for 779.0 nm is significantly larger than that for 440.9 nm.

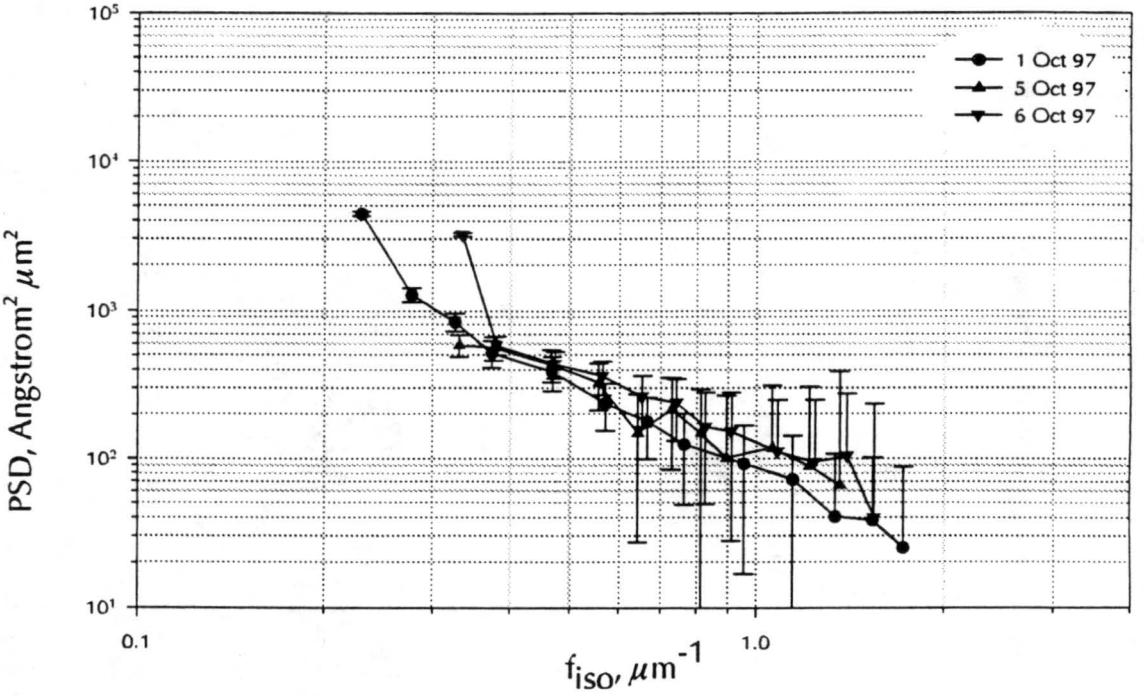

Figure 22: PSD versus f_{iso}, λ = 440.9 nm

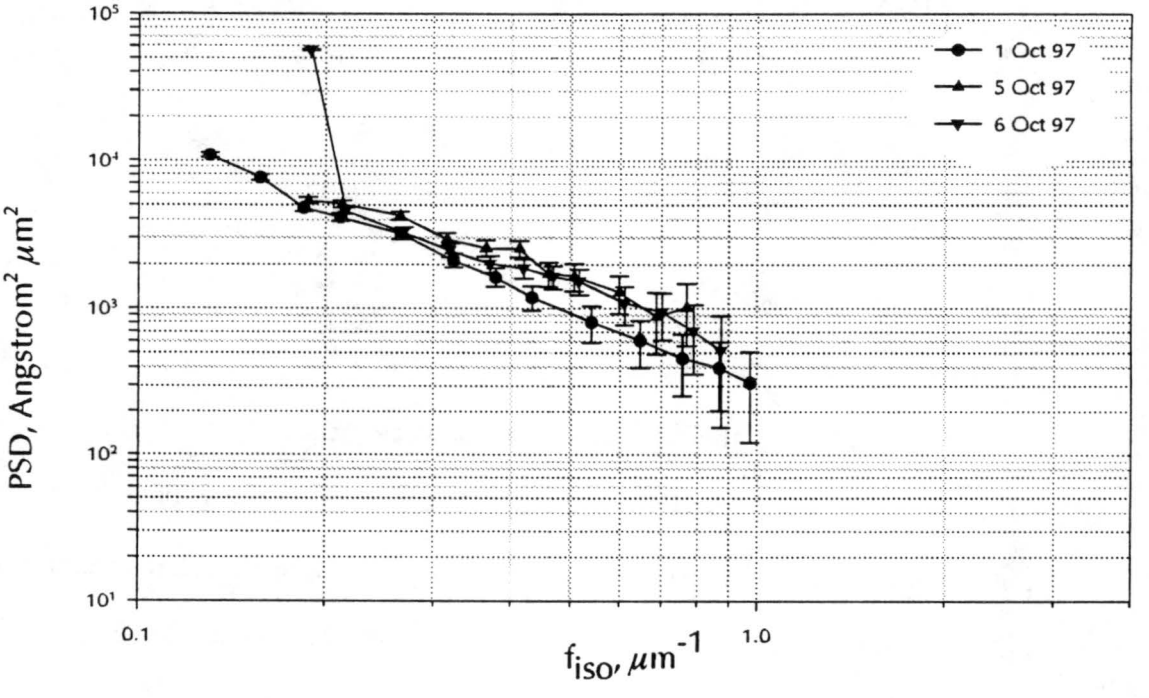

Figure 23: PSD versus f_{iso}, λ = 779.0 nm

Table 8: Values for n and K_n determined from nonlinear regression of PSD results

Case	n	Std. error for n	K_n	Std. error for K_n	r^2
λ = 440.9 nm					
1 Oct 97	2.364	0.1071	59.79	7.497	0.9925
5 Oct 97	1.519	0.1381	118.7	14.95	0.9501
6 Oct 97	1.514	0.06804	139.4	7.146	0.9862
Combined	1.928	0.09865	93.72	9.609	0.9512
λ = 779.0 nm					
1 Oct 97	1.867	0.07262	237.0	32.05	0.9928
5 Oct 97	1.205	0.07489	758.0	79.38	0.9728
6 Oct 97	1.372	0.04531	546.2	31.28	0.9922
Combined	1.535	0.05598	443.9	41.77	0.9674

7.1 *Uncertainty in Measurements*

7.1.1 Angular Position

The scattering angle calculations depend on:

- the solar azimuth and zenith angles
- the instrument position
- the azimuth and zenith angles of the mirror normal

For these calculations, the instrument position vector is assumed to be at zero degrees azimuth angle and 90 degrees zenith angle in local horizontal coordinates. The offset position vectors are taken to be those calculated at the time of each measurement, using the astronomical algorithm. The mirror normal vectors are calculated as the vectors

midway between the instrument position and the offset positions. Using these three vectors, the incident and scattering angles may be calculated.

However, the actual setup of the tracker and instrument may differ slightly from these ideals. The accuracy of the scattering angle calculations depends on how closely the initial setup of the tracker and instrument matches the assumed setup. The dominant source of error is expected to be the position of the instrument. During startup, the alignment of the tracker and the instrument can be checked by operating the tracker in mirror mode and reflecting the solar beam back toward the instrument. Good alignment is indicated if the solar beam is targeted on the instrument. If not, the process can be repeated until good alignment is obtained. This alignment was performed before the start of each day's measurements. An estimate for the uncertianty in the instrument alignment (0.38 degrees) was determined based on the size of the required adjustments and based on the results of the earlier tests of tracking accuracy. This uncertainty was assumed to apply as well to each of the calculated scattering angles.

7.1.2 Measurements and Derived Quantities

- **Mirror reflectance**

A mean value of mirror reflectance was calculated for each wavelength. The standard deviation was used to estimate the uncertainty.

- **Direct-offset signals**

The direct-offset signal was measured twice for each data set, once at the beginning of the set and once at the end. The two values were averaged to get an estimate of the direct-offset signal at the time of the mirror-offset measurements. The standard deviation of the two values was used to estimate the uncertainty.

- **Mirror-offset signals**

Replicate measurements of the mirror-offset signals were not made within each data set, so a standard deviation could not be used to estimate the uncertainty. The dominant error was expected to be due to error in angular position. The sensitivity of the mirror-offset signal to angular position was estimated for each data point, then scaled by the uncertainty in angular position.

- **Direct-solar signals**

The direct-solar signals were relatively insensitive to errors in angular position, as long as the sun was within the instrument's field of view. The signals were measured with a precision of about 0.1% for 779.0 nm and from 0.5% to 0.05%, depending on gain, for 440.9 nm. A conservative estimate of +/- 2 nA was used, amounting to about 0.2% uncertainty at 779.0 nm and 1% at 440.9 nm.

- **$\cos(\theta_s)$, $\cos(\theta_i)$**

These two functions are used in the calculation of the BRDF and PSD. The uncertainties were estimated by perturbing θ_s and θ_i by ± 0.38 degrees, then looking at the variation in the function.

- **Scattering terms, BRDF, PSD**

The uncertainties in the scattering terms, BRDF's and PSD's were determined by propagating the uncertainties through their respective calculations.

8. Discussion of Mirror Scatter Test Results

The results show that solar and background scattering contribute strongly to the mirror-offset measurements . This implies that, for this mirror, solar and background scattering would produce significant errors in radiance and irradiance measurements of diffuse skylight.

8.1 *Background Scattering*

Except for small offset angles, background scattering is a much more significant contaminant than the solar scattering. Background scatter is more difficult to predict than solar scatter, since its calculation requires the convolution of the BRDF with the background radiance field incident on the mirror. If the mirror scattering properties are not isotropic, this calculation becomes even more complicated, since the BRDF will then vary with the azimuth angle of the incident radiance.

In general, the background scatter appears to vary somewhat weakly with mirror position, with two exceptions. First, in tests A and D, $i_{scat,background}$ has a local minimum near 30 degrees offset angle with local maxima on either side. This could be due to an isolated variation in the surface profile of the mirror, *e.g*, a scratch. Note that tests A and D were both performed early in the day, while the remaining tests were performed in the afternoon. Relative to a set of coordinates fixed to the mirror, the paths traced out by the incident solar, incident target and reflected target beams are different for the two groups of tests (morning versus afternoon) (Figure 24). So it appears that, in tests A and D, an

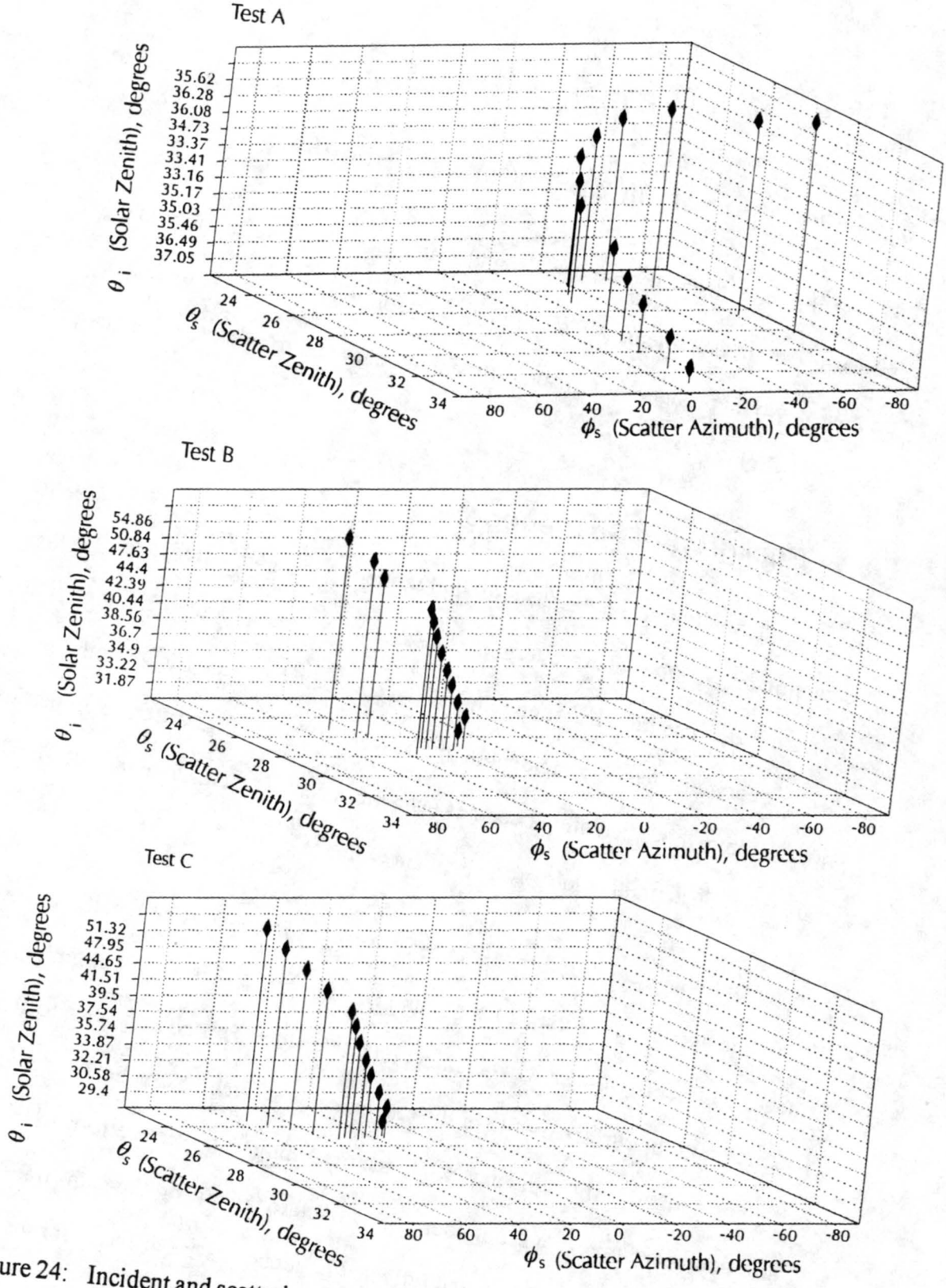

Figure 24: Incident and scattering angles for tests A, B and C. Zenith angles are relative to the mirror normal, while azimuth angles are relative to the reflected incident solar beam. Tests D, E and F are similar to A, B and C respectively.

isolated surface feature was observed and this surface feature had an effect at both short and long wavelengths.

Second, in test E, $i_{scat,background}$ has a local maximum near 22 degrees offset angle. This feature is repeated in test F at about 20 degrees offset angle. Again, this is possibly due to a surface defect. The slight differences in the magnitude and offset angle may be due to the difference in time of the observations for the two data points. The data point for test E was taken at 16:50:55 LDT, while that for test F was taken at 16:06:35 LDT. The slightly different solar and target positions would have produced a slightly different set of scattering coordinates relative to the mirror. In this case, a similar feature did not appear in the tests at 440.9 nm. The structure of the defect may have been such that it does not scatter significantly at the shorter wavelength.

A third anomalous value for background scattering occurs in test A at about 6 degrees offset angle. This was apparently a result of the unusually high value for the solar scatter at this offet angle, and is discussed in the next section.

Since $i_{scat,background}$ seems to vary weakly with offset angle, one approach to predicting $i_{scat,background}$ would be to treat it as a constant. If $i_{scat,background}$ is averaged over all measurements at 440.9 nm (n=36, excluding the anomalous value from test A at 6 degrees), the mean is $2.679 \cdot 10^{-3}$ nA with a standard deviation of $1.098 \cdot 10^{-3}$. This compares to a range for i_{spec} of $6.21 \cdot 10^{-3}$ nA to $2.33 \cdot 10^{-2}$ nA over all three tests. Among the three tests, the mean values of $i_{scat,background}$ are fairly consistent (Table 9). However, for test A, σ is of the same magnitude as the mean, while for tests B and C, σ is about an order of magnitude smaller than the mean. This suggests greater variation in the measurement of $i_{scat,background}$ in test A, though it is not clear why this is the case. As noted

Table 9: Mean and standard deviation of $i_{scat,background}$ for each test, along with the range of values for i_{spec}.

Test	Mean, $i_{scat,background}$	σ, $i_{scat,background}$	N	Range, i_{spec}
A	$2.566 \cdot 10^{-3}$	$1.829 \cdot 10^{-3}$	12	$1.18 \cdot 10^{-2}$ - $2.33 \cdot 10^{-2}$
B	$2.482 \cdot 10^{-3}$	$1.395 \cdot 10^{-4}$	12	$6.21 \cdot 10^{-3}$ - $2.24 \cdot 10^{-2}$
C	$2.987 \cdot 10^{-3}$	$5.563 \cdot 10^{-4}$	12	$8.55 \cdot 10^{-3}$ - $2.06 \cdot 10^{-2}$
D	$1.42 \cdot 10^{-2}$	$1.377 \cdot 10^{-3}$	13	$6.26 \cdot 10^{-3}$ - $3.62 \cdot 10^{-2}$
E	$4.493.10^{-3}$	$1.054 \cdot 10^{-3}$	11	$5.77 \cdot 10^{-3}$ - $4.17 \cdot 10^{-2}$
F	$5.997 \cdot 10^{-3}$	$1.257 \cdot 10^{-3}$	11	$7.18 \cdot 10^{-3}$ - $3.59 \cdot 10^{-2}$

above, test A differs from tests B and C in that the paths traced by the incident solar, incident target and reflected target beams are not the same. So it is possible that either the mirror scattering properties or the background radiance field viewed by the mirror were more variable with respect to offset angle in test A than in B and C. Although the inaccuracy introduced by using a constant, mean value for $i_{scat,background}$ would be relatively small at small offset angles, it would be significant at larger offset angles.

At 779.0 nm (n=35), the mean is $8.676.10^{-3}$ nA with a standard deviation of $4.522 \cdot 10^{-3}$. This compares to a range for i_{spec} of $5.77 \cdot 10^{-3}$ nA to $4.17 \cdot 10^{-2}$ nA. Again, the uncertainty introduced by using a single mean value for $i_{scat,background}$ would be significant at larger offset angles. In addition, there seem to be significant differences in the mean values among tests D, E and F (Table 9).

Overall, these results seem to preclude a simple analytical method or model for dealing with background scatter. Other alternatives would be to shade the mirror from the

background radiance field or obtain a mirror which would produce less scattering (*i.e.*, with a smaller BRDF). Modifications to the mirror will be discussed further in the conclusions.

8.2 *Solar Scattering*

As noted above, except for small offset angles, solar scatter is a less significant contaminant than background scatter, but is non-negligible even at larger offset angles. For 440.9 nm, the solar scatter ranged from about 10% of the total signal at small offset angles to about 1% of the total signal at offset angles near 45 degrees. For 779.0 nm, the range was from about 20% to 3%.

In some cases, at small offset angles the solar beam was incident on the objective lens of the sunphotometer even though the sun was outside the instrument's field of view (Figure 25). In earlier measurements, it was found that even if the sun was outside the sunphotometer's field of view (*i.e.*, offset angles larger than 1 degree), scattering of the solar beam by the objective lens produced an extremely strong signal. This signal overwhelmed any signal due to the diffuse field contained in the instrument's field of view. Consequently, we tried to take measurements only for those offset angles for which the objective lens was shaded from the solar beam. In some cases, the objective lens could be shaded during the direct-offset measurements, but could not be shaded during the mirror-offset measurements. This resulted in anomalously high signals for the mirror-offset measurements with normal signals for the direct-offset measurements and caused the solar scatter term to be overestimated. This appears to have occurred in test A at about 6 degrees offset angle, test C at about 8 degrees and test F at about 8 degrees. In the case of test A, the direct-offset signal was small, possibly because the diffuse target

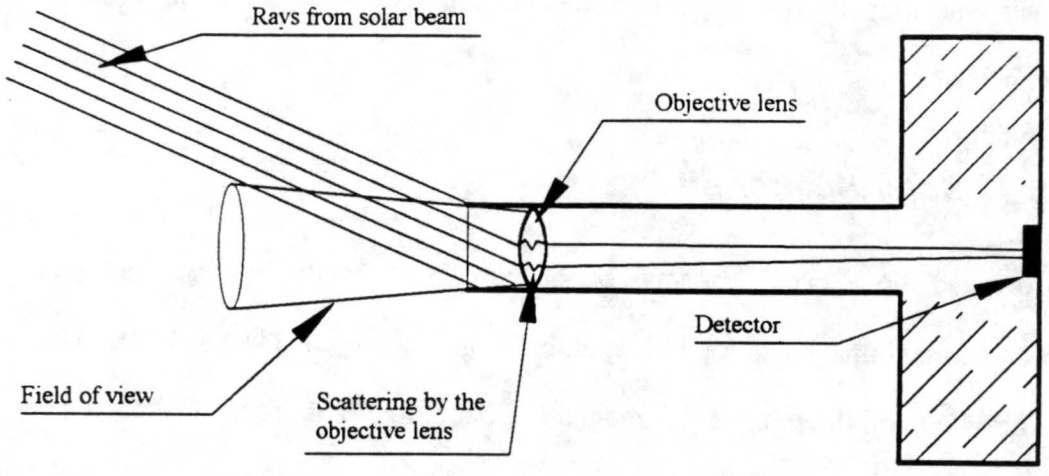

Figure 25: Sunphotometer with solar beam incident on objective lens

was partially blocked when the direct solar beam was shaded from the aperture of the sunphotometer. This led to an anomalous negative value for the background scatter.

The scaled BRDF's for 440.9 nm generally appeared to be in good agreement. This suggests that the mirror surface is relatively isotropic and that the grating equations describe the surface adequately, at least at this wavelength. At 779.0 nm, the same does not appear to be true. The BRDF for test D appears to differ systematically from tests E and F, while tests E and F appear to be in reasonably good agreement. The incident and scattering angles for tests E and F are almost the same, so the scaling should have affected the two BRDF's approximately the same. The differences between the BRDF's for tests E and F are then most likely due to measurement error. On the other hand, the incident and scattering angles for test D were significantly different than those for tests E

and F (much like the diferences shown in Figure 24). So the different BRDF results for test D are probably due to anisotropy of the mirror scattering properties (most likely) or due to problems with scaling.

The PSD's are seen to differ in a similar fashion. The regression results for individual tests show that the PSD's are fairly well predicted by an equation of the form of (22). Among tests A, B and C, the values of the parameters n and K_n for test A appear to differ systematically from those for tests B and C. Similarly, the parameters for test D appear to differ systematically from those for tests E and F. This suggests that the scattering properties of the mirror are not isotropic.

An additional feature is revealed by comparing the regression results for test A with test D, test B with test E, and test C with test F. We see that n is consistently larger for tests at 440.9 nm than for tests at 779.0 nm. Also, K_n is consistently smaller for tests at 440.9 nm than for tests at 779.0 nm. This shows that the scattering properties of the mirror do not scale with wavelength, at least for these two wavelengths, one in the visible and one in the near-IR. The implication is that the assumptions made when using Rayleigh-Rice theory to relate BRDF and PSD (that the mirror is a clean, optically smooth, front surface reflector) are not valid for at least one of these wavelengths.

A number of causes might have contributed to this problem. First, to meet the smoothness requirement, the amplitude of variations in surface height should be less than a wavelength and the surface slope must be less than one (Stover, 1990). This is a relatively inexpensive mirror and may not meet this requirement. In addition, there are some visible defects in the mirror surface. Second, the mirror was being used in a somewhat windy, dusty environment. The mirror was cleaned with a lens brush between

tests, but this may not have been sufficient. Third, the mirror may not have been performing entirely as a front surface reflector. Stover (1990) suggests that, at longer wavelengths, scattering may be affected by subsurface defects. This mirror also has a protective coating which may have interfered with front-surface reflection.

Testing the mirror over a range of wavelengths and under more controlled conditions might allow the cause to be identified. For example, if a test at 500 nm produced a PSD similar to that for 440.9 nm, while a test at 779.0 nm produced a dissimilar one, one might narrow the cause to subsurface defects. In the end, it might be possible to find a relationship by which solar scatter could be predicted.

An alternate approach would be to specify a mirror with a reduced BRDF, such that solar scatter, and perhaps background scatter as well, would be insignificant compared to the desired signal. As can be seen in equations (23) and (25), if the BRDF is reduced by a constant fraction, the scattered radiances are reduced by the same fraction.

9. Conclusions

9.1 *Compensation for Misalignment*

The performance of the correction algorithm is most strongly influenced by the accuracy and timing of the iterative corrections. Improved performance was achieved when multiple iterative corrections were made in clusters distributed over the day. Multiple corrections made at nearly the same time appear to reduce the potential random variation in tracking error, much as replicate measurements reduce the random error in a measurement. Spacing corrections over several hours keeps the tracking error more stable over time.

9.2 *System Performance*

With highly accurate manual corrections, the accuracy of the solar tracker could approach 0.1 degrees. Three factors affect the accuracy of the solar tracker: the accuracy of the solar position calculation, the accuracy of the electromechanical system, and the accuracy of the correction algorithm. The solar position is calculated to an accuracy near 0.02 degrees and the accuracy of the electromechanical system is near 0.075 degrees. Simulation of the correction algorithm showed that it was capable of correcting for tracker misalignment to within two times the standard deviation of the iterative corrections. If the errors in the iterative corrections could be minimized, the accuracy of the tracker could approach 0.1 degrees, primarily due to errors in the solar position calculation and the electromechanical system.

Field testing of the tracker showed an average tracking error of 0.11 degrees over a two day period when a correction scheme as described above was used with very accurate manual corrections. Tracking errors ranged from 0.06 degrees to 0.17 degrees. The accuracy of the iterative corrections was estimated as 0.04 degrees.

9.3 *Mirror Mode Performance*

In the mirror mode of observing solar radiances, the scattering by the mirror of both the direct solar beam and the diffuse background radiance was found to have a significant impact on measurements of diffuse skylight. For many of the measurements, background scatter was larger than solar scatter. Background scatter ranged from a minimum of about 20% of the mirror-offset signal to maximum values of 40% (440.9 nm) and 70% (779.0 nm). Solar scatter ranged from minimum values of 1% (440.9 nm) and 3% (779.0 nm) for large offset angles, to maximum values of 10% (440.9 nm) and 20% (779.0 nm) for small offset angles.

Because of the significance of background scatter, it must be controlled if measurements of diffuse skylight are to be made when operating in the mirror mode. One option is to predict the background scatter and remove it from the measurement. A second option is to reduce it to less significant values, either by shading the mirror from the diffuse background radiance field or by improving the scattering properties of the mirror.

Background scatter is difficult to predict because of the complexity of its relationship with the incident radiance field and the mirror scattering properties. A simple approach in which background scatter is treated as a constant with respect to offset angle was unacceptable due to the size of the uncertainty in the constant value. There was some

evidence that the background scatter was influenced by defects in the mirror surface and that the scattering properties of the mirror were not isotropic. It is possible that a less-damaged or higher quality mirror would give more acceptable results.

Scattering properties for the mirror were calculated from solar scatter data. These results also suggest that the mirror scattering properties are not isotropic, and that the scattering properties do not scale with wavelength between the tested visible and near-IR wavelengths. Since the scattering properties do not scale with wavelength, the Rayleigh-Rice relation between BRDF and PSD is not valid for at least one of these wavelengths, and possibly both. In that case, one or both of the PSD's calculated here are in error. Further testing at other wavelengths would be required to determine if there is a range of wavelengths over which Rayleigh-Rice theory could be applied.

Shading the mirror would reduce or eliminated the unwanted incident light. The shade would need to have a port through which an instrument could view the mirror, or the instrument would have to be located inside the shade. An additional port would be required through which the mirror could view the target, and this port would have to move to follow the target position. The requirement that the shade move with the target complicates this approach.

A third approach would be to obtain a mirror with smaller magnitudes of scattering than were found for this mirror. For example, a uniform 90% reduction in the BRDF at 440.9 nm would give background scatter of 2% to 4% and solar scatter of 0.1% to 1%. Published BRDF data for front-surface aluminum mirrors suggest that this performance could be achieved (Stover, 1990), at least at visible wavelengths (the particular wavelength used to test the mirror is not shown, but many of the other tests Stover

describes are at 632.8 nm). The performance of the mirror would have to be verified over the range of wavelengths of interest.

10. References

Aerotech, Inc., 1991: *Electro-Optical Product Guide*, Aerotech, Inc., Pittsburgh, 224 pp.

Bretagnon, P. and G. Francou, 1988: "Planetary theories in rectangular and spherical variables," *Astronomy and Astrophysics*, **202**, 309-315.

Kincaid, D. and W. Cheney, 1991: *Numerical Analysis: Mathematics of Scientific Computing*, Brooks/Cole Publishing Co., Pacific Grove, CA, 690 pp.

Kneizys, F. X., L. W. Abreu, G. P. Anderson, J. H. Chetwynd, E. P. Shettle, A. Berk, L. S. Bernstein, D. C. Robertson, P. Acharya, L. S. Rothman, J. E. A. Selby, W. O. Gallery, S. A. Clough, 1996: *The MODTRAN 2/3 Report and LOWTRAN 7 Model*, U. S. Air Force Phillips Laboratory, Geophysics Directorate, Hanscomb Air Force Base, MA, 200 pp.

Liou, K.-N., 1990: *An Introduction to Atmospheric Radiation*, Academic Press, Inc., San Diego, CA, 392 pp.

Meeus, J., 1991: *Astronomical Algorithms*, Willmann-Bell, Inc., Richmond, VA, 429 pp.

Motion Engineering, Inc., 1990: *Exerciser Software, DirectLibrary™ Software, Version 3.4*, Motion Engineering, Inc., Santa Barbara, CA, diskette.

Nautical Almanac Office, U. S. Naval Observatory, 1991: *The Air Almanac 1992*, U. S. Government Printing Office, Washington, D. C., 906 pp.

Newmann, W. M., and R. F. Sproull, 1979: *Principles of Interactive Computer Graphics*, McGraw-Hill Book Company, New York, 541 pp.

Nicodemus, F. E., J. C. Richmond, J. J. Hsia, I. W. Ginsberg and T. Limperis, 1977: *Geometrical Considerations and Nomenclature for Reflectance*, U.S. Department of Commerce, National Bureau of Standards, Washington, 52 pp.

Press, W. H., S. A. Teukolsky, W. T. Vetterling, and B. P. Flannery, 1992: *Numerical Recipes in C: The Art of Scientific Computing*, Cambridge University Press, Cambridge, 994 pp.

Råde, L. and B. Westergren, 1990: *Beta Mathematics Handbook*, CRC Press, Boca Raton, FL, 494 pp.

Sax, J., 1991: *Astronomical Algorithms "C" Software Toolbox*, Willmann-Bell, Inc., Richmond, VA, diskette.

Stover, J. C., 1990: *Optical Scattering: Measurement and Analysis*, McGraw-Hill, Inc., New York, 238 pp.

Van Huffel, S. and J. Vandewalle, 1991: *The Total Least Squares Problem: Computational Aspects and Analysis*, Society for Industrial and Applied Mathematics, Philadelphia, 300 pp.

Wood, N. B., S. K. Cox and C. L. Cornwall, 1996: *Atmospheric Science Paper No. 604, An Improved Solar Tracking System with Linear Regression Error Correction*, Colorado State University, Fort Collins, CO, 46 pp.

11. Appendix A

Excerpts from *Atmospheric Science Paper No. 604, An Improved Solar Tracking System with Linear Regression Error Correction*

Operation of the Solar Tracker

A1.1 Overview

The solar tracker control program contains routines to calculate the true solar coordinates, to allow the user to manually correct the tracker position, to calculate from those corrections a transformation matrix which transforms the true solar coordinates to the applied solar coordinates in the tracker's coordinate system, and to allow the user control over the program and the mount.

A1.2 Preliminary Set Up

The two-axis mount is attached to a table and connected to the computer and amplifiers as shown in Figure 3. The table should be near level and the mount should be positioned pointing south. Looking through the scope, the user can manually adjust the gimbal position to sight on a permanent landmark.

A1.3 Starting the program

The user then starts the program, TRACK1.EXE. The tracking program displays an information screen describing the program and asks whether or not to continue. Next the program enters the manual correction mode. The user manually adjusts the gimbal position to point directly south (zero point) or to the sun. Then the user initializes the tracker's position by either setting the zero point (directly south) or, if the mount is pointed at the sun, by having the computer calculate the zero point from the solar position along with the known site location and local time. This causes the computer to store the servo motor encoder values that correspond to the tracker's zero position.

Once initialized, the program switches to run mode and begins tracking along the expected solar path. This path will not match the actual solar path unless the tracker is perfectly aligned meridionally and is on a perfectly level plane.

A1.4 Program Modes

A1.4.1 Run Mode

This mode is the normal operating mode for the solar tracker software. In Run mode, the program retrieves the current time from the PC clock, and calculates the true solar coordinates. If the transformation matrix is activated (see section A1.5.2.5 Select Matrix below), these coordinates are transformed through the matrix. Then the new position information is sent to the motor controller, and the numerical displays on the screen are

updated. These displays include site parameters (latitude, longitude, altitude, and time zone), time and date, calculated solar position, calculated mount position, and the mount positioning error.

A1.4.2 Manual Correct Mode

Once the device is in Run mode, corrections can be made using the Manual Correct mode.

Once a manual correction is completed and the tracker is aligned with the current solar position, the user presses the **S** key. This enters the correction data into memory and updates the correction matrix. The program then returns to Run mode.

After three or more corrections are entered, the program is capable of calculating a transformation matrix for the current setup. Once the transformation matrix is activated, the program processes its true solar coordinates through this matrix before outputing them to the motor control software.

A1.4.3 Graphics Display Mode

The Graphics Display mode is similar to Run mode, except without the numerical displays. Instead, the screen displays the day's calculated solar path, and the position of the mount relative to the path. The horizontal axis of the graph is azimuth, the vertical axis is elevation, and both axes are labelled in degrees.

This mode is useful when a solar offset is being used. The user can watch a sinusoidal offset represented graphically on the screen as the tracker sweeps out the path.

A1.5 Program Options

A1.5.1 File Menu

The file menu allows users to perform various functions of saving and retrieving data from disk. The filenames for save and load operations are hardcoded into the program. For example, when the "Save Site and Correction Data" option is selected, the computer writes file RESTART.DAT. This is the same filename written upon exit. If the user wishes to retain the previous file, the DOS Command option can be used to copy one file to another.

A1.5.2 Parameter Menus

Various parameters may be changed while the program is running. These include the site parameters, the current local time and date, the motor control parameters, the solar offset variables, and the correction matrix selection. Each of these options is included in the Main Menu while in Run mode. Examples of these menus appear in the appendix.

A1.5.2.1 Edit Site

The site editing menu is used for setting the correct values of the site parameters longitude, latitude, altitude and timezone offset from GMT.

A1.5.2.2 Edit Time and Date

This menu is used to enter corrections to the current local time and date. When entered, these corrections update the PC's clock and calendar.

A1.5.2.3 Edit Motor

The user can change the values of motor control variables like gain, pole and zero using this menu. The values can be changed for each axis of motion. This should only be attempted by a knowledgeable user, as it can cause problems with the motors. If a gain value is too large, the motor could vibrate. A gain too small could cause a large positioning error, or a complete lack of movement.

A1.5.2.4 Solar Offset

The tracker is capable of tracking a known angle off the sun. There are two methods of doing this: a time offset, and a sinusoidal offset in azimuth and/or elevation. If a time offset is used, the tracker will move to the position on the solar path corresponding to the present time plus the offset. The offset may be negative, to allow tracking behind the sun. The angular value of an offset of five minutes will vary depending on time of day and day of year.

To implement a sinusoidal offset, the user must enter an amplitude in degrees and a frequency in sec^{-1}. The angular offset is then added to the appropriate axis (azimuth or elevation). A frequency of 0.1 sec^{-1} will yield a period of 20π seconds (approximately one minute and three seconds).

The equation used to calculate the offset is:

$$F = M*cos\ (\omega t) \qquad \text{(A1)}$$

where F is the number of degrees to add to the azimuth or elevation, M is the maximum amplitude of the offset, ω is the frequency as described above, and t is the number of seconds since 0:00 local time.

A1.5.2.5 Select Matrix

This menu selection allows the user to choose which matrix is used for transforming the calculated solar coordinates. The choices are: none, regression matrix, and manual matrix. After selecting the manual matrix, the user has the option of manually inputing the matrix. Alternately, the user could load the manual matrix from the file MATRIX.DAT using the File Menu "Load Matrix" command.

Examples of Program Status Screens

```
                    Solar Tracker Control Program
Direct                 Status:  Running....                  Matrix OFF N 13
+-------------------------------------------------------------------------+
|          Site Parameters                    |  Local Time and Date      |
|  Lat:  40.5833        Lng:  105.1250        |  Time:  08:05:03.92       |
|  Alt:   1568.00 m     Timezone: +6.00 to UT |  Date:  07 Apr 1994       |
|-------------------------------------------------------------------------|
|  Solar Position  |  Gimbal Position     Counter  |      Error            |
|  AZ:  -85 03'30" |  AZ: -85 03'30"      -51034   |      +0               |
|  EL:  +16 18'04" |  EL: +16 18'04"      +9780    |      +0               |
|-------------------------------------------------------------------------|
|                                                                         |
|                                                                         |
|                                                                         |
|                                                                         |
|-------------------------------------------------------------------------|
|                              Main Menu                                  |
|  P - Pause/Resume      E - Edit Motor          D - Mirror/Direct        |
|  Q - Quit              C - Manual Correct      I - Reinitialize         |
|  S - Edit Site         V - View Matrices       M - Select Matrix        |
|  T - Edit Time/Date    O - Solar Offset        F - File Menu            |
|  G - Graphics Disp     N - Redraw Screen                                |
+-------------------------------------------------------------------------+
```

Screen 1 is an example of a typical screen during Run Mode. The upper left corner indicates Mirror or Direct operation. Under the program name is the operational mode (Initializing, Running or Paused). The upper right corner contains the matrix correction information. The matrix status (ON or OFF) is followed by a letter indicating which matrix is in use (N = none, R = Regression, M = Manually input matrix). The number following shows how many correction points are currently in memory.

The upper left box contains the site data being used in the solar calculations. These values may be changed by hitting the S key, for the Edit Site option. Latitude and longitude are given in degrees, positive to the North and West. Altitude is in meters. Time zone is represented in the number of hours added to local time to equal GMT.

The upper right box displays the current local time and date, which may be changed by hitting the T key.

The second row of boxes contains position information. The leftmost box shows the calculated solar position. The next box displays the current command position for the two-axis mount. (This will be different from the solar position when a correction matrix is being used, or when a correction offset is in place.) This box also displays the command position in encoder counts. (600 counts = 1°.) The rightmost window then displays the motor position error (command position - actual position) in encoder counts.

The middle window is for user interaction with the various menu commands. During normal operation, it remains blank unless a user command is being performed.

The lower window shows the keys used to activate various user commands. Some of these commands work instantly (**Q**uit, **P**ause, **G**raphics display, Redraw Scree**N**, **D**irect/Mirror toggle) while others access a separate routine for displaying or inputing new data (**E**dit Site, **E**dit Time/Date, **E**dit Motor, **V**iew Matrices, Solar **O**ffset, **S**elect Matrix). Still other commands access other menus (Manual **C**orrect, Re**I**nitialize, **F**ile Menu).

```
                    Solar Tracker Control Program
Direct                 Status:  Paused                  Matrix OFF N 13
+-------------------------------------------------------------------------+
|            Site Parameters                          | Local Time and Date
|  Lat:  40.5833          Lng:  105.1250              | Time:  08:06:11.42
|  Alt:   1568.00 m       Timezone: +6.00 to UT       | Date:  07 Apr 1994
|-------------------------------------------------------------------------
|  Solar Position    | Gimbal Position     Counter  |      Error
|  AZ:  -84 52'12"   | AZ: -84 52'12"      -50921   |       +0
|  EL:  +16 30'51"   | EL: +16 30'51"      +9908    |       +0
|-------------------------------------------------------------------------
|                    Select Option from File Menu
|
|
|
|
|-------------------------------------------------------------------------
|                              File Menu
|    S - Save Site Parameters and Correction Data to RESTART.DAT
|    L - Load Site Parameters and Correction Data from RESTART.DAT
|    C - Clear Correction Memory        R - Regr matrix -> RMATRIX.DAT
|    D - Execute DOS Command            M - Manu matrix <- MATRIX.DAT
|    Q - return to main menu
+-------------------------------------------------------------------------+
```

Screen 2 shows the program screen as it appears after the **F** key has been pressed to activate the File Menu. The lower window now displays the File Menu options, including **Save** startup data (site parameters and previously entered correction data) to file RESTART.DAT, **Load** startup data from RESTART.DAT, **Clear** all previously entered corrections from memory, execute a **DOS** command, save a calculated **Regression** matrix to file RMATRIX.DAT, load a **Matrix** from file MATRIX.DAT to the manually entered matrix, and **Quit** the File Menu.

```
                    Solar Tracker Control Program
Direct                    Status:  Paused                    Matrix OFF N 13
+-------------------------------------------------------------------------+
|            Site Parameters                  |  Local Time and Date      |
|  Lat:  40.5833          Lng:  105.1250      |  Time:  08:07:05.74       |
|  Alt:   1568.00 m       Timezone: +6.00 to UT  Date:  07 Apr 1994       |
|-------------------------------------------------------------------------|
|  Solar Position  |  Gimbal Position     Counter  |      Error            |
|  AZ:  -84 43'06" |  AZ: -84 43'06"      -50830   |      +0               |
|  EL:  +16 41'07" |  EL: +16 41'07"      +10011   |      +0               |
|-------------------------------------------------------------------------|
|                          Site Parameters                                |
|                                                                         |
|      Latitude  = 40.5833              Longitude = 105.1250              |
|      Altitude  = 1568.0 m             Time Zone = 6.00                  |
|                                                                         |
|          Are these values correct? (y/n)                                |
|-------------------------------------------------------------------------|
|                            Main Menu                                    |
|  P - Pause/Resume      E - Edit Motor          D - Mirror/Direct        |
|  Q - Quit              C - Manual Correct      I - Reinitialize         |
|  S - Edit Site         V - View Matrices       M - Select Matrix        |
|  T - Edit Time/Date    O - Solar Offset        F - File Menu            |
|  G - Graphics Disp     N - Redraw Screen                                |
+-------------------------------------------------------------------------+
```

Screen 3 is an example of pressing the S key while in Run Mode. If the user answers No, the program will display each parameter in turn, prompting the user to accept the present value or enter a new value. Then the program will again display all four parameters, prompting the user with this screen until the user accepts the parameters.

```
                    Solar Tracker Control Program
Direct                    Status:  Paused                    Matrix OFF N 13
+-------------------------------------------------------------------------+
|            Site Parameters                  |  Local Time and Date      |
|  Lat:  40.5833        Lng:  105.1250        |  Time:  08:08:20.82       |
|  Alt:   1568.00 m     Timezone: +6.00 to UT |  Date:  07 Apr 1994       |
|-------------------------------------------------------------------------|
|  Solar Position  |  Gimbal Position    Counter  |     Error             |
|  AZ:  -84 30'30" |  AZ: -84 30'30"     -50704   |     +0                |
|  EL:  +16 55'20" |  EL: +16 55'20"     +10153   |     +0                |
|-------------------------------------------------------------------------|
|                      Manual Motor Adjustment                            |
|                                                                         |
|   Direction: None                    AZ:    -50704                      |
|   # Steps:   1                       EL:    10153                       |
|   Status:    Done                                                       |
|                                                                         |
|-------------------------------------------------------------------------|
|                          Correction Menu                                |
|  Set step size (1 to 100000) using F1(10), F2(100), F3(1000), F4(10000) |
|      <Shift> F1(-10), F2(-100), F3(-1000), F4(-10000)                   |
|  Up/Down/Left/Right Arrows move <step size> units in that direction     |
|  Z,S - reset motor counters to zero or solar position                   |
|  Q - return to main menu, ignore changes                                |
+-------------------------------------------------------------------------+
```

Screen 4 shows the Manual Correction Mode, accessed from Run Mode by pressing the C key. In this mode, the user can use the function keys (F1 through F4) and the arrow keys to move the two-axis mount to a desired location (the corrected solar position, or the zero position on startup or reinitialization). Each move requires two steps: setting the step size for the move, and entering the direction for the move. Using the function keys, the user can specify a step size from 10 to 100,000 steps. (There are 216,000 steps per revolution for each stage of the mount.) Pressing function keys in sequence will add the corresponding step size to the total step size, displayed in the middle window. To add negative step sizes, hold down the Shift key while pressing one of the function keys.

Once the desired step size is displayed, the user simply presses one of the arrow keys to enter the direction for the move. The mount will then move to the appropriate position. The up arrow corresponds to an increase in elevation angle. The right arrow will turn the mount clockwise (as viewed from the top).

Example: To move the unit 22010 steps toward the west (clockwise), the user would press the following sequence of keys: F4 F4 F3 F3 F1 <right arrow>

Once the desired position is attained, the user enters either S or Z, depending on whether they have aligned the tracker with the sun or with the zero azimuth/zero elevation point. The program will then enter Run Mode.

To quit without saving any correction data, the user enters Q. The program will return to Run Mode.

```
                    Solar Tracker Control Program
Direct                      Status:  Paused                    Matrix OFF N 13
+-------------------------------------------------------------------------------+
|              Site Parameters                  |  Local Time and Date          |
|  Lat:  40.5833          Lng:  105.1250        |  Time:  08:09:15.42           |
|  Alt:   1568.00 m       Timezone: +6.00 to UT |  Date:  07 Apr 1994           |
|-------------------------------------------------------------------------------|
|  Solar Position  |  Gimbal Position     Counter  |      Error                  |
|  AZ:  -84 21'19" |  AZ: -84 21'19"      -50613   |      +0                     |
|  EL:  +17 05'40" |  EL: +17 05'40"      +10256   |      +0                     |
|-------------------------------------------------------------------------------|
|                  Select Matrix Correction Mode:                               |
|                                                                               |
|                        1 - No Correction                                      |
|                        2 - Regression Matrix                                  |
|                        3 - Manually Input Matrix                              |
|                                                                               |
|-------------------------------------------------------------------------------|
|                              Main Menu                                        |
|  P - Pause/Resume      E - Edit Motor        D - Mirror/Direct                |
|  Q - Quit              C - Manual Correct    I - Reinitialize                 |
|  S - Edit Site         V - View Matrices     M - Select Matrix                |
|  T - Edit Time/Date    O - Solar Offset      F - File Menu                    |
|  G - Graphics Disp     N - Redraw Screen                                      |
+-------------------------------------------------------------------------------+
```

Screen 5 shows the matrix selection screen, which is entered from Run Mode by pressing the M key. The user selects which matrix to use by pressing 1, 2 or 3 on the keyboard. To exit without changing matrices, press **<ESC>**.

```
                    Solar Tracker Control Program
Direct                    Status:  Running....                  Matrix ON  R 13
+-------------------------------------------------------------------------------+
|          Site Parameters                          | Local Time and Date       |
|  Lat:  40.5833          Lng:  105.1250            | Time:  08:10:20.84        |
|  Alt:   1568.00 m       Timezone: +6.00 to UT     | Date:  07 Apr 1994        |
|-------------------------------------------------------------------------------|
|  Solar Position  |  Gimbal Position     Counter    |      Error                |
|  AZ:  -84 10'18" |  AZ: -90 00'09"      -54001     |       +0                  |
|  EL:  +17 17'33" |  EL:  +8 12'00"      +4920      |       +0                  |
|-------------------------------------------------------------------------------|
|                                                                               |
|                                                                               |
|                                                                               |
|                                                                               |
|-------------------------------------------------------------------------------|
|                              Main Menu                                        |
|  P - Pause/Resume       E - Edit Motor          D - Mirror/Direct             |
|  Q - Quit               C - Manual Correct      I - Reinitialize              |
|  S - Edit Site          V - View Matrices       M - Select Matrix             |
|  T - Edit Time/Date     O - Solar Offset        F - File Menu                 |
|  G - Graphics Disp      N - Redraw Screen                                     |
+-------------------------------------------------------------------------------+
```

Screen 6 shows the display as it appears when a correction matrix has been selected. Notice the upper right corner, where the word ON now appears, followed by the letter R, to indicate that the Regression matrix is being used. The number after the "R" still indicates the number of correction points currently in memory.

```
                    Solar Tracker Control Program
Direct                      Status:  Paused                    Matrix ON  R 13
+-------------------------------------------------------------------------------+
|            Site Parameters                    |  Local Time and Date          |
|  Lat:  40.5833          Lng:  105.1250        |  Time:  08:11:00.82           |
|  Alt:   1568.00 m       Timezone: +6.00 to UT |  Date:  07 Apr 1994           |
|-------------------------------------------------------------------------------|
|  Solar Position  |  Gimbal Position     Counter  |      Error                  |
|  AZ:  -84 03'34" |  AZ: -89 53'31"      -53935   |      +0                     |
|  EL:  +17 25'36" |  EL:  +8 19'51"      +4998    |      +0                     |
|-------------------------------------------------------------------------------|
|                        Current Rotation Matrix                                |
|                                                                               |
|       Regression      1.6369012444   0.4371250033   1.0693262691              |
|                       0.0045506460   1.0126871865  -0.0159713361              |
|                      -0.5188726390  -0.3484803751   0.0966309162              |
|                  <Hit Any Key To Continue>                                    |
|-------------------------------------------------------------------------------|
|                              Main Menu                                        |
|  P - Pause/Resume      E - Edit Motor          D - Mirror/Direct              |
|  Q - Quit              C - Manual Correct      I - Reinitialize               |
|  S - Edit Site         V - View Matrices       M - Select Matrix              |
|  T - Edit Time/Date    O - Solar Offset        F - File Menu                  |
|  G - Graphics Disp     N - Redraw Screen                                      |
+-------------------------------------------------------------------------------+
```

Screen 7 is the display after hitting the V key to View the matrices. The displayed matrix is an example of a regression matrix calculated from thirteen correction points.

```
                    Solar Tracker Control Program
Direct                    Status:  Running....                  Matrix ON  R 13
+-------------------------------------------------------------------------------+
|          Site Parameters                          | Local Time and Date       |
|  Lat:  40.5833          Lng:  105.1250            | Time:  08:13:10.56        |
|  Alt:   1568.00 m       Timezone: +6.00 to UT     | Date:  07 Apr 1994        |
|-------------------------------------------------------------------------------|
|  Solar Position   | Gimbal Position     Counter        | Error                |
|  AZ:  -83 41'39"  | AZ: -88 46'14"      -53262   T     | +0                   |
|  EL:  +17 50'07"  | EL:  +9 39'20"      +5793    T     | +0                   |
|-------------------------------------------------------------------------------|
|                                                                               |
|                                                                               |
|                                                                               |
|                                                                               |
|-------------------------------------------------------------------------------|
|                              Main Menu                                        |
|  P - Pause/Resume        E - Edit Motor          D - Mirror/Direct            |
|  Q - Quit                C - Manual Correct      I - Reinitialize             |
|  S - Edit Site           V - View Matrices       M - Select Matrix            |
|  T - Edit Time/Date      O - Solar Offset        F - File Menu                |
|  G - Graphics Disp       N - Redraw Screen                                    |
+-------------------------------------------------------------------------------+
```

Screen 8 shows the program running with the regression matrix on, and a time offset in use. The letter T appearing after the counter positions indicates that azimuth and elevation are being affected by the Time Offset.

(A time offset can be used to move the solar tracker forward or backward along the solar path. This is useful for taking readings close to, but not directly on, the sun.)

```
                    Solar Tracker Control Program
Direct                    Status:  Running....                  Matrix ON  R 13
+-------------------------------------------------------------------------------+
|            Site Parameters                          |  Local Time and Date    |
|  Lat:  40.5833          Lng:  105.1250              |  Time:  08:13:59.33     |
|  Alt:   1568.00 m       Timezone: +6.00 to UT       |  Date:  07 Apr 1994     |
|-------------------------------------------------------------------------------|
|  Solar Position    |  Gimbal Position      Counter          |     Error         |
|  AZ:  -83 33'24"   |  AZ: -89 25'39"       -53656           |     +0            |
|  EL:  +17 59'19"   |  EL:  +7 28'50"       +4488     S      |     +0            |
|-------------------------------------------------------------------------------|
|                                                                               |
|                                                                               |
|                                                                               |
|                                                                               |
|-------------------------------------------------------------------------------|
|                                  Main Menu                                    |
|  P - Pause/Resume        E - Edit Motor          D - Mirror/Direct            |
|  Q - Quit                C - Manual Correct      I - Reinitialize             |
|  S - Edit Site           V - View Matrices       M - Select Matrix            |
|  T - Edit Time/Date      O - Solar Offset        F - File Menu                |
|  G - Graphics Disp       N - Redraw Screen                                    |
+-------------------------------------------------------------------------------+
```

Screen 9 shows the program running with the regression matrix on, and a sinusoidal offset in use. The letter S appearing after the elevation counter position indicates that the elevation is being affected by the Sine Wave Offset.

(A sine wave offset can be used to move the solar tracker in a sinusoidal path centered on the sun. Separate magnitudes and periods can be set for the offsets along the azimuth and elevation directions.)

```
                    Solar Tracker Control Program
Direct                    Status:  Paused                    Matrix OFF N 13
+-------------------------------------------------------------------------+
|          Site Parameters                    | Local Time and Date       |
|  Lat:  40.5833        Lng:  105.1250        | Time:  08:15:39.84        |
|  Alt:   1568.00 m     Timezone: +6.00 to UT | Date:  07 Apr 1994        |
|-------------------------------------------------------------------------|
|  Solar Position  | Gimbal Position    Counter |      Error              |
|  AZ:  -83 16'21" | AZ: -83 16'21"     -49963  |        +0               |
|  EL:  +18 18'18" | EL: +18 18'18"     +10983  |        +0               |
|-------------------------------------------------------------------------|
|                      Motor Parameters: AZ                               |
|                                                                         |
|                          Gain = 64                                      |
|                    Maximum Velocity = 10                                |
|                      Acceleration = 2                                   |
|              Are these values correct? (y/n)                            |
|-------------------------------------------------------------------------|
|                           Main Menu                                     |
|  P - Pause/Resume      E - Edit Motor          D - Mirror/Direct        |
|  Q - Quit              C - Manual Correct      I - Reinitialize         |
|  S - Edit Site         V - View Matrices       M - Select Matrix        |
|  T - Edit Time/Date    O - Solar Offset        F - File Menu            |
|  G - Graphics Disp     N - Redraw Screen                                |
+-------------------------------------------------------------------------+
```

Screen 10 is an example of the Motor Parameter Editing screen, accessed from Run Mode by pressing the **E** key. The routine is similar to that for editing the site parameters.

```
                    Solar Tracker Control Program
Direct                 Status:  Running....                Matrix ON  R 13
+-------------------------------------------------------------------------+
|            Site Parameters                  |  Local Time and Date      |
|  Lat:  40.5833        Lng:  105.1250        |  Time:  08:13:59.33       |
|  Alt:   1568.00 m     Timezone: +6.00 to UT |  Date:  07 Apr 1994       |
|-------------------------------------------------------------------------|
|  Solar Position  |  Gimbal Position    Counter        |     Error       |
|  AZ:  -83 33'24" |  AZ: -89 25'39"     -53656         |     +0          |
|  EL:  +17 59'19" |  EL:  +7 28'50"     +4488    S     |     +0          |
|-------------------------------------------------------------------------|
|                                                                         |
|                                                                         |
|                                                                         |
|                                                                         |
|-------------------------------------------------------------------------|
|                              Main Menu                                  |
|  P - Pause/Resume      E - Edit Motor          D - Mirror/Direct        |
|  Q - Quit              C - Manual Correct      I - Reinitialize         |
|  S - Edit Site         V - View Matrices       M - Select Matrix        |
|  T - Edit Time/Date    O - Solar Offset        F - File Menu            |
|  G - Graphics Disp     N - Redraw Screen                                |
+-------------------------------------------------------------------------+
```

Screen 9 shows the program running with the regression matrix on, and a sinusoidal offset in use. The letter S appearing after the elevation counter position indicates that the elevation is being affected by the Sine Wave Offset.

(A sine wave offset can be used to move the solar tracker in a sinusoidal path centered on the sun. Separate magnitudes and periods can be set for the offsets along the azimuth and elevation directions.)

```
                    Solar Tracker Control Program
Direct                    Status:  Paused                    Matrix OFF N 13
+-------------------------------------------------------------------------+
|          Site Parameters                  | Local Time and Date         |
|  Lat:  40.5833      Lng:  105.1250        | Time:  08:15:39.84          |
|  Alt:   1568.00 m   Timezone: +6.00 to UT | Date:  07 Apr 1994          |
|-------------------------------------------------------------------------|
|  Solar Position  | Gimbal Position    Counter |      Error              |
|  AZ:  -83 16'21" | AZ: -83 16'21"     -49963  |      +0                 |
|  EL:  +18 18'18" | EL: +18 18'18"     +10983  |      +0                 |
|-------------------------------------------------------------------------|
|                      Motor Parameters: AZ                               |
|                                                                         |
|                           Gain = 64                                     |
|                     Maximum Velocity = 10                               |
|                       Acceleration = 2                                  |
|                Are these values correct? (y/n)                          |
|-------------------------------------------------------------------------|
|                           Main Menu                                     |
|  P - Pause/Resume      E - Edit Motor          D - Mirror/Direct        |
|  Q - Quit              C - Manual Correct      I - Reinitialize         |
|  S - Edit Site         V - View Matrices       M - Select Matrix        |
|  T - Edit Time/Date    O - Solar Offset        F - File Menu            |
|  G - Graphics Disp     N - Redraw Screen                                |
+-------------------------------------------------------------------------+
```

Screen 10 is an example of the Motor Parameter Editing screen, accessed from Run Mode by pressing the E key. The routine is similar to that for editing the site parameters.

```
                    Solar Tracker Control Program
Direct                 Status:  Paused                    Matrix OFF N 13
+-------------------------------------------------------------------------+
|          Site Parameters                  |  Local Time and Date        |
|  Lat:  40.5833        Lng:  105.1250      |  Time:  08:17:05.69         |
|  Alt:   1568.00 m     Timezone: +6.00 to UT |  Date:  07 Apr 1994       |
|-------------------------------------------------------------------------|
|  Solar Position  |  Gimbal Position     Counter  |      Error            |
|  AZ:  -83 01'45" |  AZ: -83 01'45"      -49817   |      +0               |
|  EL:  +18 34'30" |  EL: +18 34'30"      +11145   |      +0               |
|-------------------------------------------------------------------------|
|                        Solar Offset Function                            |
|                                                                         |
|   Select (0) for no offset, (1) Time Offset or (2) Az/El Offset:        |
|                                                                         |
|                                                                         |
|-------------------------------------------------------------------------|
|                             Main Menu                                   |
|  P - Pause/Resume      E - Edit Motor        D - Mirror/Direct          |
|  Q - Quit              C - Manual Correct    I - Reinitialize           |
|  S - Edit Site         V - View Matrices     M - Select Matrix          |
|  T - Edit Time/Date    O - Solar Offset      F - File Menu              |
|  G - Graphics Disp     N - Redraw Screen                                |
+-------------------------------------------------------------------------+
```

Screen 11 shows the Offset Selection screen. Pressing the O key from Run Mode will activate this screen. The user can choose a method of tracking off of the sun by selecting the appropriate number 0, 1 or 2.

A Time Offset will cause the tracker to move to a point ahead of (or behind) the current solar position on the solar path. The user specifies the time offset in hours, minutes and seconds. The angular displacement of a particular time differential will vary depending on date and time of day.

```
                    Solar Tracker Control Program
Direct                    Status:  Paused                    Matrix OFF N 13
+-------------------------------------------------------------------------+
|          Site Parameters                  |  Local Time and Date        |
|  Lat:  40.5833        Lng:  105.1250      |  Time:  08:17:05.69         |
|  Alt:   1568.00 m     Timezone: +6.00 to UT |  Date:  07 Apr 1994       |
|-------------------------------------------------------------------------|
| Solar Position  | Gimbal Position     Counter  |      Error               |
| AZ:  -83 01'45" | AZ: -83 01'45"      -49817   |      +0                  |
| EL:  +18 34'30" | EL: +18 34'30"      +11145   |      +0                  |
|-------------------------------------------------------------------------|
|                        Solar Offset Function                            |
|                                                                         |
|     Time Offset = 00:00:00                                              |
|  where a time of 5 minutes equals an angle of 1.25 degrees (early       |
|  or late) to 1.66 degrees (at noon), depending on the date and time.    |
|          Is this value correct? (y/n)                                   |
|-------------------------------------------------------------------------|
|                            Main Menu                                    |
|  P - Pause/Resume      E - Edit Motor        D - Mirror/Direct          |
|  Q - Quit              C - Manual Correct    I - Reinitialize           |
|  S - Edit Site         V - View Matrices     M - Select Matrix          |
|  T - Edit Time/Date    O - Solar Offset      F - File Menu              |
|  G - Graphics Disp     N - Redraw Screen                                |
+-------------------------------------------------------------------------+
```

Screen 12 shows the Time Offset Parameter screen, where the user enters a value for the time differential, and a direction (positive or negative) for the offset.

```
                    Solar Tracker Control Program
Direct                    Status:  Paused                    Matrix OFF N 13
+-------------------------------------------------------------------------+
|            Site Parameters                  | Local Time and Date       |
|  Lat:  40.5833        Lng:  105.1250        | Time:  08:19:23.99        |
|  Alt:   1568.00 m     Timezone: +6.00 to UT | Date:  07 Apr 1994        |
|-------------------------------------------------------------------------|
|  Solar Position  | Gimbal Position    Counter |      Error              |
|  AZ:  -82 38'10" | AZ: -82 38'10"     -49581  |      +0                 |
|  EL:  +19 00'35" | EL: +19 00'35"     +11405  |      +0                 |
|-------------------------------------------------------------------------|
|                                                                         |
|                  Do you really want to quit? (y/n)                      |
|                                                                         |
|              Do you wish to move the mount to zero? (y/n)               |
|                                                                         |
|                                                                         |
|-------------------------------------------------------------------------|
|                              Main Menu                                  |
|  P - Pause/Resume      E - Edit Motor          D - Mirror/Direct        |
|  Q - Quit              C - Manual Correct      I - Reinitialize         |
|  S - Edit Site         V - View Matrices       M - Select Matrix        |
|  T - Edit Time/Date    O - Solar Offset        F - File Menu            |
|  G - Graphics Disp     N - Redraw Screen                                |
+-------------------------------------------------------------------------+
```

Screen 13 is the screen as it appears just before exiting the program. When the user selects Q from the Main Menu during Run Mode, the program prompts the user to confirm the desire to quit. If this is answered affirmatively, the program prompts whether or not to return the mount to the zero position. This is usually desirable, placing the mount in the correct position to start the program again later.